Aus der Universitätsklinik für Hals-, Nasen und Ohrenheilkunde
mit Poliklinik Tübingen

Sektion Physiologische Akustik und Kommunikation

Endocytosis and Transcytosis in the Outer Hair Cell of the Guinea Pig Cochlea

**Inaugural-Dissertation
zur Erlangung des Doktorgrades
der Medizin**

**der Medizinischen Fakultät
der Eberhard Karls Universität
zu Tübingen**

vorgelegt von

Klenske, Entcho Marianov

2021

Aus der Universitätsklinik für Hals-, Nasen und Ohrenheilkunde
mit Poliklinik Tübingen

Sektion Physiologische Akustik und Kommunikation

Endocytosis and Transcytosis in the Outer Hair Cell of the Guinea Pig Cochlea

**Inaugural-Dissertation
zur Erlangung des Doktorgrades
der Medizin**

**der Medizinischen Fakultät
der Eberhard Karls Universität
zu Tübingen**

vorgelegt von

Klenske, Entcho Marianov

2021

Dekan: Prof. Dr. rer. nat. Bernd Pichler

1. Berichterstatter: Prof. Dr.-Ing. Anthony W. Gummer

2. Berichterstatter: Prof. Dr. med. Dr. rer. nat. Fritz Schick

3. Berichterstatter: Prof. Dr. Claus-Peter Richter

Tag der Disputation: 09.11.2021

Widmung

An meine beruflichen und menschlichen Vorbilder: meinem Großvater und Namensvetter Prof. Dr. Entcho Kalchev sowie meiner Mutter Dr. Julia Klenske

Contents

List of abbreviations

A	apical
Ach	acetilcholine
AEE	apical early endosome
Aff	afferent
AP	adapter protein
ARE	apical recycling endosome
a.u.	arbitrary units
AU	Airy unit
BEE	basal early endosome
BM	basilar membrane
ConA	concanavalin A
CRE	common recycling endosome
Da	Dalton
DIC	differential interference contrast
$DiOC_6$	3,3′-dihexyloxacarbocyanine iodide
DMSO	dimethyl sulphoxide
Eff	efferent
ER	endoplasmic reticulum
FI	fluorescence intensity
FM1-43	N-(3-Triethylammoniumpropyl)-4-(4(Dibutylamino) Styryl) Pyridinium Dibromide
FM4-64	N-(3-Triethylammoniumpropyl)-4-(6-(4-(Diethylamino) Phenyl) Hexatrienyl) Pyridinium Dibromide
GABA	gamma-aminobutyric acid
HB	hair bundle
HBSS	Hanks' balanced salt solution
HEPES	N-2-Hydroxyethylpiperazine-N′-2-ethanesulfonic acid
IC	infracuticular
IHC	inner hair cell
IM	inframiddle

IN	infranuclear
M	middle
MET	mechanoelectrical transduction
Mon	monastrol
MVBs	multivesicular bodies
MW	molecular weight
NA	numerical aperture
OHC	outer hair cell
PAO	phenylarsine oxide
PBS	phosphate buffered salt solution
PM	plasma membrane
ROI	region of interest
SD	standard deviation
SN	supranuclear
SSC	subsurface cisternae
TIP	2,4,6-Triiodophenol
TM	tectorial membrane

1 Introduction

1.1 General introduction

Uptake of foreign material inside cells is essential for cells to deliver substances to their required cellular destinations. Various uptake mechanisms, traffic pathways as well as transport proteins participate in these processes. In epithelial cells, the uptake and traffic mechanisms have already been investigated and described.
However in the outer hair cell (OHC), a bipolar epithelial cell, there is a sparsity of data as to what processes are involved in uptake and transport along the cell. While the apical pole has been a more intense research focus over the past years, the basal pole of the cell has just recently become a subject of research interest. Nevertheless, there is no consensus until now as to which types of internalization are prevalent at each pole. Furthermore, the transport pathways and motor proteins involved in traffic inside the OHC have not yet been fully investigated.
Therefore, this study attempts to elucidate the main uptake processes and transport pathways in the OHC. For visualization of these processes, confocal laser scanning microscopy was used. For determining which types of uptake exist at each pole, uptake blockers of different types of internalization were applied. In order to clarify the traffic pathways and motor proteins, various transport blockers were utilized.
In the following sections the necessary theoretical background of this study is elaborated.

1.2 Hair Cells

Hair cells located in the organ of Corti (Figure 1) are responsible for transduction of auditory signals into neural impulses located in the mammalian cochlea. There are two types of hair cells: the IHCs, which are purely sensory cells and the OHCs, which have both sensory and motoric functions. The etymology of hair cells derives from the apically located stereocilia, which are motile cilia that look like tiny hairs, on the apical surface of the cell. There are approximately 3,500 IHCs, 12,000 OHCs and numerous supporting cells along the approximately 35-mm long human cochlea (Spoendlin, 1972). Allthough OHCs and IHCs differ in function, both show similar morphological structures. Specifically, they are both bipolar cells, where the apical pole possesses a hair bundle bathing in endolymph, while the basolateral cell membrane is surrounded by perilymph.

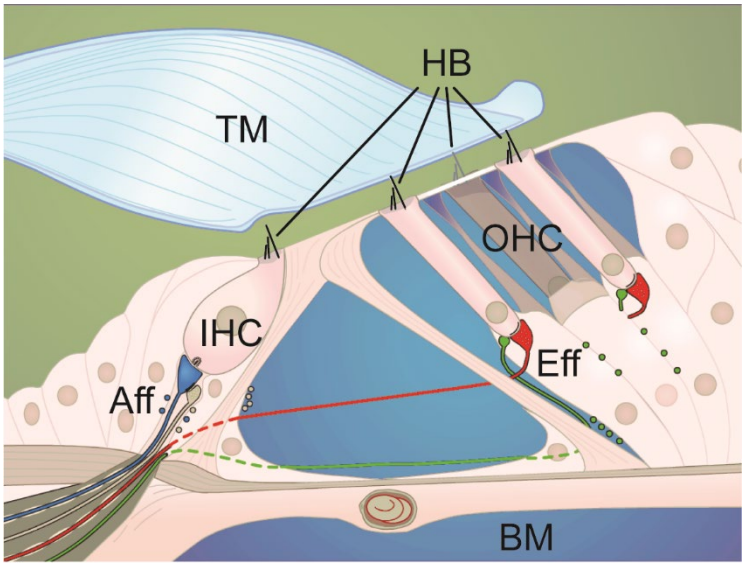

Figure 1. Organ of Corti

Illustration of the three rows of outer hair cells (OHC) and one row of inner hair cell (IHC). The tectorial membrane (TM) is located above the hair cells and below them is the basilar membrane (BM). IHCs mostly possess afferent nerve fibres (Aff) while the OHCs are innervated mostly by efferent nerve fibres (Eff). /Modified from www.cochlea.eu/.

1.2.1 Inner hair cells (IHCs)

IHCs are the sensory cells of the organ of Corti and possess a goblet-shape structure. Each IHC has stereocilia arranged in line on its apical surface, the cuticular plate. The tips of the longest stereocilia are not attached to the tectorial membrane (TM, Figure 1). The IHC body is filled with round mitochondria, Golgi apparatus, multivesicular bodies, lysosomes, and a well-developed endoplasmatic reticulum. At the apex of the cell there is a high concentration of microtubules, whereas in the body of the IHC microtubule-concentration decreases. IHCs possess 95% of afferent innervations of hair cells. These nerve fibres are responsible for forwarding nerve impulses towards the brain. At the reticular lamina, IHCs form tight junctions with supporting cells, such as Hensen's cells or Deiters' cells. Another characteristic of IHCs is that through these supporting cells, IHCs have the possibility of intracellular communication via Ca^{2+} signalling (Mammano *et al.*, 2007).

1.2.2 Outer hair cells (OHCs)

In contrast to the purely sensory IHCs, OHCs have motoric functions and possess a cylindrical, elongated shape (Figure 2). At the cuticular plate, each OHC has stereocilia arranged in a typical "W" shape and connects to supporting cells with tight junctions. The apical surface is composed of circumferantly oriented actin filaments and a microtubule network, which is less in density than in IHCs. Along the basolateral plasma membrane of the OHC, several layers of membranous sacs, called the subsurface cisternae (SSC), are located. The number of SSCs layers is species dependant, e.g. one layer in humans (Arnold & Anniko, 1990) vs. multiple layers in guinea pig (Saito, 1983). Between the plasma membrane and the SSCs there are layers of pillar-like structures. Below the cuticular plate of the OHC a lamellar structure called Hensen's body, consisting of concentric layers of membrane similar to the SSCs, is located. Mitochondria are organized along the SSCs parallel to the lateral wall of the cell and in a central strand running in the middle of the cell. A quite unique structural property of OHCs is their well-developed endoplasmic reticulum (ER), whose function is not yet clearly understood. The nucleus of the OHC is located near the base, where the afferent and efferent synapses are stationed. The neurotransmitters associated with this synaptic region are acetylcholine (Ach) and γ-aminobutric acid (GABA) (Plinkert *et al.*, 1989).

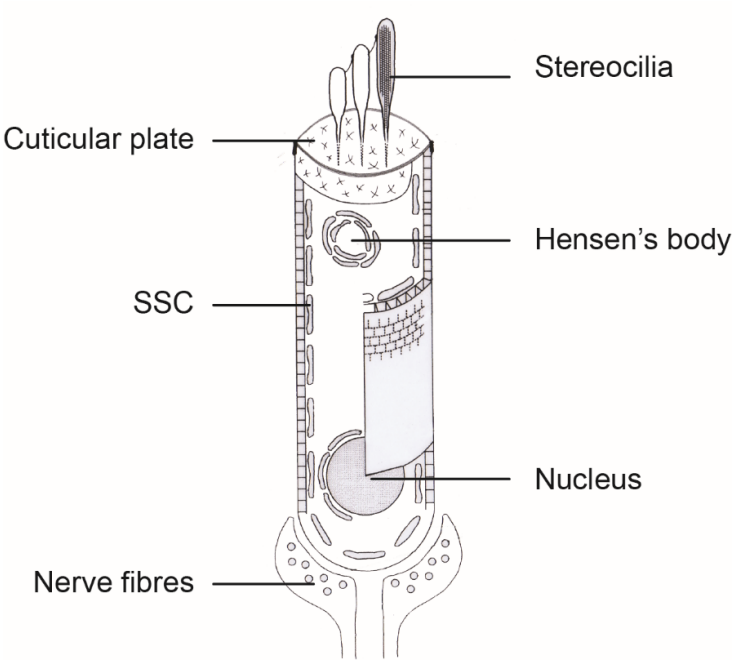

Figure 2. Morphology of the OHC

Schematic diagram showing the cell organelles inside of an OHC. Note the presence of an elaborated SSC-system around the nucleus and the lateral plasma membrane of the cell. /With kind permission from Prof. S. Preyer/.

1.2.3 Functional role of hair cells

The functional importance of hair cells is defined by their being responsible for the transformation of vibrations into a neural signal, which is then transmitted to the brain. Vibrations of the tympanic membrane are transmitted to the *Scala vestibuli* by the ossicles creating pressure differences between *Scala vestibuli* and *Scala tympani*. This pressure difference displaces the basilar membrane and, with it, the organ of Corti (von Békésy, 1960). The displacement of the basilar membrane evokes a shearing motion between the tectorial membrane and the basilar membrane that excites the hair cells by deflecting their hair bundles. Deflection of the hair bundle in the direction of the longest stereocilia stretches tip links, which are part of the gating apparatus of the mechanoelectrical transduction (MET) channels, forming a mechanical link between the top of the shorter cilium where the MET channels are located (Harasztosi & Gummer, 2008; Beurg *et al.*, 2009) and the

lateral membrane of the longer adjacent cilium. Therefore, stereocilia deflection towards the longest cilia causes the MET channels to open. Through these nonspecific cation channels, potassium and calcium ions enter the stereocilia, which are driven by the electrochemical gradient of these ions between the extracellular (endolymph) and the intracellular space. The positively charged ion-entry depolarizes the plasma membrane of hair cells (Hudspeth, 1989). The change of transmembrane potential caused by deflection of the hair bundle is called the receptor potential.

In IHCs, in the true sensory cells of the cochlea, depolarization opens voltage-gated Ca^{2+} channels in the basolateral membrane, resulting in Ca^{2+} influx, which leads to transmitter release. The coding of depolarization into action potentials is conducted via the release of the neurotransmitter glutamate due to a Ca^{2+}-dependent interaction with SNARE-proteins, which lead to the fusion of transmitter-containing vesicles with the presynaptic cell membrane (Safieddine & Wenthold, 1999).

In OHCs, depolarization and hyperpolarization cause the soma, respectively, to contract and elongate (Brownell *et al.*, 1985; Kachar *et al.*, 1986; Zenner, 1986). The key to the function of OHCs as electromechanical transducers is the motor protein, called prestin (Zheng *et al.*, 2000). Prestin (SLC26A5) is member A5 of the SLC26/SulP anion transporter family and is expressed in the basolateral membrane (Kalinec *et al.*, 1992) at a high density (Huang & Santos-Sacchi, 1993). In addition to contraction, depolarization also results in neurotransmitter release (LeMasurier & Gillespie, 2005).

1.3 Endocytosis

Endocytosis (Greek: *endo*- inside, *cyto*- cell, *osis*- condition) is defined as the process by which a eukaryotic cell internalizes material from the extracellular environment. The reciprocal process of ejecting intracellular material to the extracellular space is known as exocytosis (Greek: *exo*- outside). These processes are clearly mutually linked and together are referred to as membrane recycling.

1.3.1 Fundamental principles of endocytosis

The plasma membrane of cells is a selective barrier, which cannot be surpassed by macromolecules. However, it is necessary for cells to adjust the composition of the plasma membrane and the intracellular compartments. Therefore, through the processes of endocytosis and exocytosis, cells regulate the entry and exit of molecules. This process of selective entry into a given area in order to lead to a specific biochemical reaction, was described as early as 1894 by Emil Fischer as the "lock and key'' principle. Although there are different types of endocytosis, they all have three major steps in common: 1) recognition of the part of the plasma membrane, 2) invagination and 3) vesicle formation. In eukaryotic cells, there is a constant forming of vesicles which transport the membrane components and internalized molecules (Alberts *et al.*, 2015). These transporting vesicles are referred to as cargo. Differentiation of the different types of endocytosis can be made by the size of the internalized membrane, vesicle ingredients and types of involved proteins. In terms of the vesicle-size, there are two main types of endocytosis: **phagocytosis** (Greek: *phago*- eating) where large particles or even other cells > 250 nm are ingested, and **pinocytosis** (Greek: *pino*- drinking) where fluids and solutes < 100 nm are ingested. The vesicles responsible for internalization of material via phagocytosis are called phagosomes, whereas the vesicles involved in pinocytosis pinosomes. Different types of phagocytosis have been described based on the types of particles and involved receptors. The most relevant for humans is the type of phagocytosis involved in the immune system to ingest "invading" cells, e.g. macrophages which ingest foreign material, debris or microbes. For pinocytosis, four different types are described: macropinocytosis, clathrin-mediated endocytosis, calveolae-mediated

endocytosis and clathrin- or calveolae-independent endocytosis (Miaczynska & Stenmark, 2008).

1. **Macropinocytosis**: A phagocytosis-like form of endocytosis, where the material is internalized by large invaginations (Figure 3). This type of endocytosis mediates the non-selective uptake of nutrients, solutions and antigens (Lim & Gleeson, 2011). The physiological role for this type of internalization is for example: nutrient uptake of the intestinal epithelia (Nunez *et al.*, 1996) and antigen internalization in macrophages and dendritic cells (Lim & Gleeson, 2011).

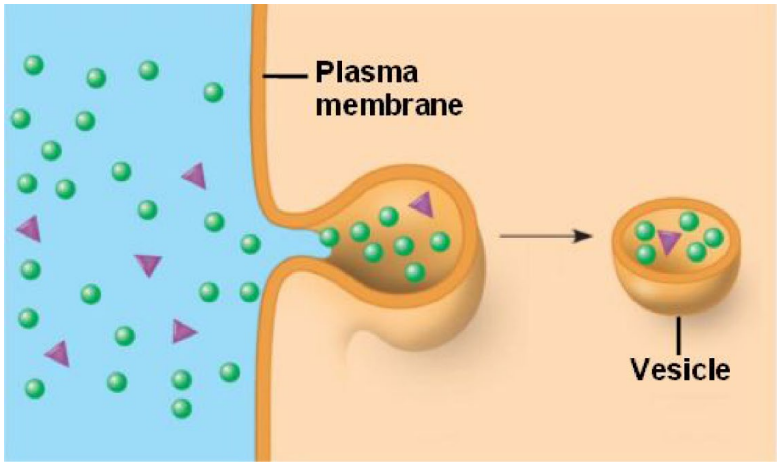

Figure 3. Pinocytosis

During pinocytosis vesicles are formed from the plasma membrane and transferred to the cytoplasm. The vesicles take up molecules (circles and triangles) from the extracellular space. /Adapted from www.biologyexams4u.com/.

2. **Clathrin-mediated endocytosis (CME)**: A form of endocytosis where the invagination is driven by a clathrin-coated vesicle (Figure 4), where clathrin is a protein in a triskelion shape with three light chains and three heavy chains (Kirchhausen *et al.*, 1987a; Kirchhausen *et al.*, 1987b). Several different adapter proteins, like dynamin, are necessary to form the clathrin coat (Traub, 2003). This pathway is used not only for molecule internalization, but also for entry of toxins (botulinum-toxin, tetanus toxin), viruses (hep C virus) and bacteria (Matteoli *et al.*, 1996; Helle & Dubuisson, 2008).

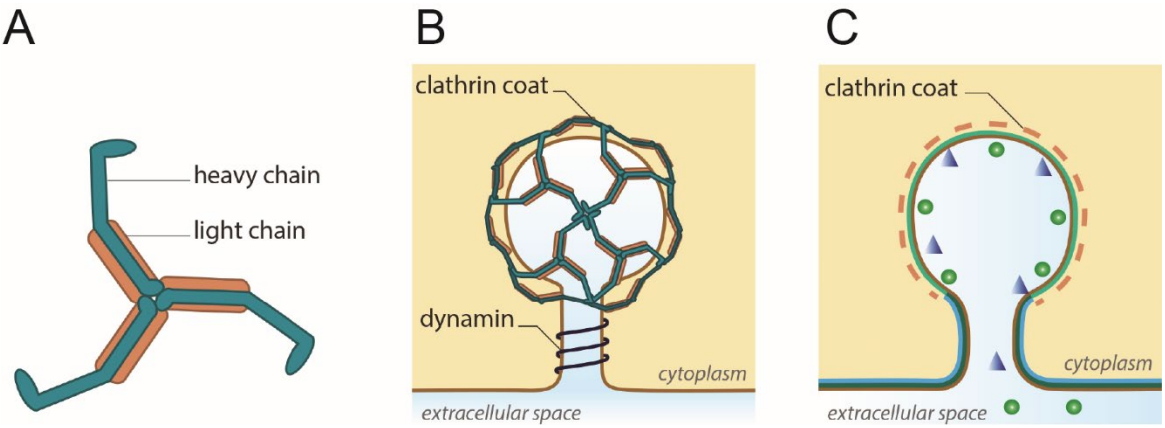

Figure 4. Clathrin-mediated endocytosis

(A) Schematic diagram showing the composition of a clathrin molecule, possessing three heavy and three light chains. (B) Diagram showing the mechanism by which a clathrin coat is formed with the aid of dynamin. (C) Clathrin-coated vesicle with internalized molecules (green circles and blue triangles). Molecules can be also seen in the extracellular space. /Adapted from www.mechanobio.info/.

3. **Clathrin-independent endocytosis**: In this type of endocytosis the vesicle formation is driven by caveolae, which are 50-90 nm large invaginations of the plasma membrane, made up of one of the three forms of the caveolin-protein-family (Rothberg *et al.*, 1992). Although this type of internalization has been extensively investigated in the past, the physiological role of caveolin-mediated endocytosis is not yet clearly defined.

4. **Clathrin- or caveolin-independent endocytosis:** Recently other types of endocytosis, which are neither clathrin nor caveolin-dependent, have been subject of research. It is thought that in these types of endocytosis other proteins such as Flotilin or small GTPase (RhoA) are essential for the internalization (Xu *et al.*, 2008).

1.3.2 Endocytosis in hair cells

In IHCs, various studies have been conducted regarding the endocytic and exocytic activities at the synaptic pole (Moser & Beutner, 2000; Beutner *et al.*, 2001; Griesinger *et al.*, 2002). At the apical pole of the IHC, the Ca^{2+} dependent endocytosis of the fluorescent dye FM1-43 and its transportation towards the synaptic pole of the cell was visualized (Griesinger *et al.*, 2002). This kinesin-dependent dye transportation towards the synaptic pole of the cell suggested that apical endocytosis regulates the synaptic membrane recycling. That study also demonstrated that the fluid phase-marker Lucifer Yellow presented a similar staining pattern to FM1-43. At the basal pole, the kinetics of exocytosis and endocytosis were observed and quantified during continuous Ca^{2+} and polarization changes (Moser & Beutner, 2000). The initial membrane recycling rate at the synapse of IHC was found to be high at the beginning, but already after a few milliseconds started to decrease. Furthermore, Ca^{2+} dependency of endocytosis and exocytosis at the IHC afferent synapse has been shown (Beutner *et al.*, 2001). One of the latest findings at the basal pole of the IHC was the verification of the coupling of otoferlin, a transmembrane protein associated with genetic hearing loss, to the adapter protein complex (AP-2), thereby influencing Ca^{2+} dependent CME (Duncker *et al.*, 2013). At the synaptic pole of the IHC, or even generally at synapses, additional types of endocytosis to the previously mentioned exist, namely "*bulk*"-and "*kiss and run*"-endocytosis. These types have differences in kinetics, i.e. have slow and fast endocytosis rates (Wu *et al.*, 2007; Smith *et al.*, 2008). However, a concrete classification of which types interact at the synapse is not yet agreed upon.

In **OHCs**, the cells investigated in this study, endocytic vesicles in the synaptic zone have been demonstrated using electron microscopy (Nadol, 1983), as well as the presence of coated vesicles and small vacuoles using horseradish peroxidase staining (Siegel & Brownell, 1986). The apical pole has been a more intense object of interest compared to the basal pole. At the infracuticular pole, the time-dependent staining pattern of the fluorescent marker FM1-43 was shown (Meyer *et al.*, 2001). Endocytosed vesicles were found to traffic rapidly to compartments along the lateral wall and to distinct intracellular compartments with an apical uptake rate of 0.8 mm^2/s (Griesinger *et al.*, 2004). Later it was reported that apically endocytosed vesicles traffic not only to different intracellular compartments, but also to the basolateral wall and the infranuclear pole (Kaneko *et al.*, 2006). Moreover, the Ca^{2+}-

dependency as well as the voltage dependency on the internalization was shown. However, “in these studies dye was applied to the extracellular environment around the apical pole of the cell, meaning that the pole of dye entrance could not be controlled” (Harasztosi *et al.*, 2014). In the meantime, a study of endocytic activity at the synaptic pole of the isolated OHC has been conducted (Harasztosi *et al.*, 2014). The uptake rate at apex and base were compared and found to be similar. As these studies show, there seems to be a certain symmetry in the dynamics of apical and basal endocytosis. Further experiments are needed to elaborate and understand the physiological function of apical as well as basal endocytosis in OHCs.

1.4 Transcytosis

Transcytosis (Greek: *tran*- through, *cyto*- cell, *osis*- condition) is defined as the process in which a eukaryotic cell transports internalized cargo along the cell towards different intracellular compartments.

1.4.1 Fundamental principles

Inside eukaryotic cells, transport of cargo to certain intracellular locations is essential for delivering biochemically active substances to their required destination. It is a way of selectively transporting material between two different environments while maintaining the distinct compositions of those environments (Tuma & Hubbard, 2003). The transport of membrane along the cell with the aid of vesicles is conducted via the cytoskeleton mainly in two different pathways: the **microtubule** pathway and the **actin filament** pathway. These pathways consist of their structure proteins tubulin and actin which polymerize to polar filaments with a minus and a plus end. In polarized epithelial cells, such as OHCs and IHCs, it is known that different active transport processes are activated when apically or basally endocytosed molecules enter the cell. Upon internalization, the cargo is delivered to the apical early endosome (AEE) or the basal early endosome (BEE), respectively. From there it is thought that cargoes can recycle to the cell surface, be delivered to the multivesicular bodies (MVBs), from which they will be delivered to lysosomes, or they can be delivered to the common recycling endosome (CRE). Cargoes leaving this intracellular compartment can be transported to the basolateral surface or through the apical recycling endosome (ARE) to the apical surface (Apodaca *et al.*, 2012).

Microtubules are tubular polymers of tubulin with an outer diameter of 20-30 nm and a total length of up to 50 µm (Figure 5). Contrary to most eukaryotic cells, where the minus end of the microtubule is located in the centre of the cell, in polarized epithelial cells the minus end is facing towards the apex (Bacallao *et al.*, 1989; Meng *et al.*, 2008). The cargo transport can be mediated in both directions by kinesin (Endow & Higuchi, 2000) and towards the minus end by dynein (Bhabha *et al.*, 2016). In polarized epithelial cells, microtubules are thought to be involved in

transport from BEE/AEE to late endosomes and from AEE to ARE (Apodaca, 2001a).

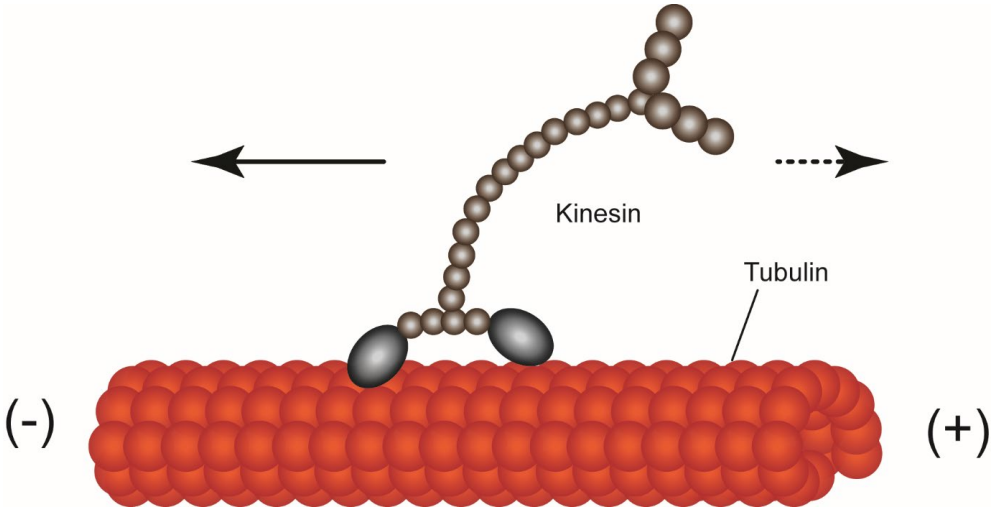

Figure 5. Microtubules

Microtubules are composed of tubulin molecules in a tubular structure. Kinesin is responsible for cargo movement along the microtubules.

Actin filaments, also known as microfilaments, are linear polymers of actin with a diameter of ~6 nm and a length of several micrometres (Figure 6). Microfilaments are responsible for transport of internalized cargo across long distances as well as short distances with the ultimate goal to reach a given intracellular location (Langford, 1995). In the OHC, actin filaments are not only found inside the cell body as part of the cytoskeleton, but also in the stereocilia at the apical pole of the cell. The motor protein associated with transport of the cargo along the microfilaments is myosin. At least 18 different forms of myosin, distinguishable by their order of amino acid sequences in the motor domain, exist out of which class I, class V, class VI and class VII have been associated with transport to the different organelles of the epithelial cell (Tuxworth & Titus, 2000). **Myosin VI** has a unique property compared to the other classes of myosin, namely that it is responsible for the transport of cargo towards the minus end of the microfilament (Wells *et al.*, 1999). In eukaryotic cells, it is believed that the plus end of microfilaments is oriented towards the plasma membrane of the cell (Cramer, 1999). Therefore, it stands to reason that myosin VI is responsible for the transport away from the plasma membrane and away from

internal organelles (Buss *et al.*, 2002; Buss *et al.*, 2004). In polarized epithelial cells, microfilaments are thought to be involved in transport from plasma membrane to AEE/BEE, from there to CRE and to the apical/basal surface (Apodaca, 2001a).

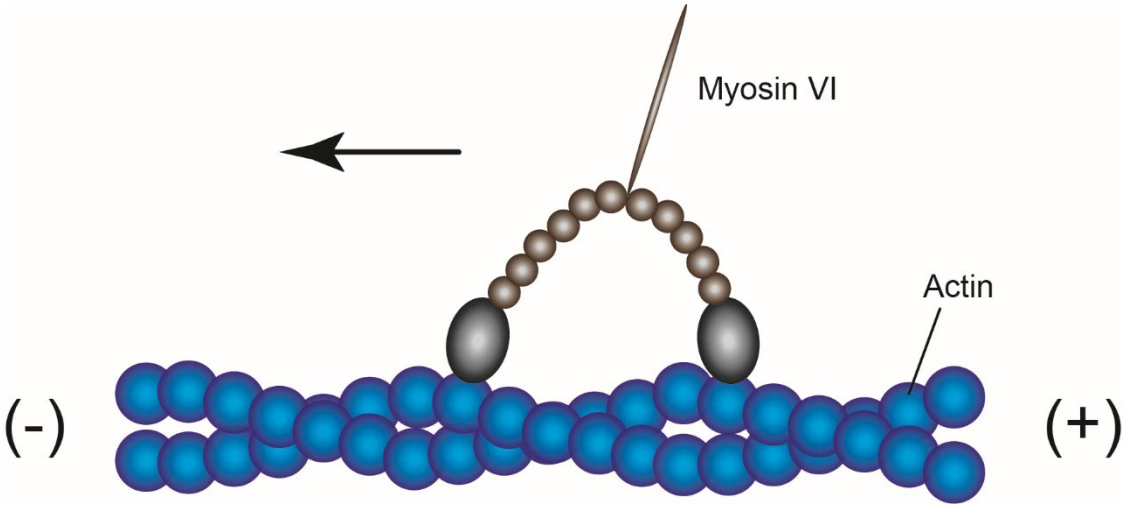

Figure 6. Microfilaments

Microfilaments are composed of actin molecules which are aligned to form a double helical structure. Myosin VI is capable of moving along the actin chain by changing its conformation; it transports cargo towards the minus end of the actin filaments.

1.4.2 Transcytosis in outer hair cells

So far little is known of the transport processes, the intracellular destinations and the motor proteins involved in transcytosis of endocytosed vesicles in OHCs. Vesicles endocytosed at the apical pole were found to traffic towards different intracellular compartments, e.g. the apical endosome, apical compartment, central compartment, lateral compartment and the basal compartment (Griesinger *et al.*, 2004). After application of the fluorescent membrane marker FM1-43, staining was first observed within ~60 s in the apical endosome, a structure responsible for fluid-phase uptake in epithelial cells. The fluid phase marker Lucifer Yellow was also applied to the apical pole of OHCs and staining was similar to that of the FM1-43. It was concluded that apically endocytosed vesicles traffic towards the apical endosome of the cell, as a first destination after internalization. In later studies regarding the apical endocytic activity in OHCs, fluorescent FM1-43 staining was shown at Hensen's body, the

basolateral wall and at the infranuclear pole of the cell (Kaneko *et al.*, 2006). The transport speed was calculated to be 0.36 μm/s. It was concluded that the transport to these intracellular destinations was along microtubules, since their concentration at the infracuticular pole was high in OHCs and the calculated speed consistent with transport speed along the microtubules. At the basal pole of OHCs, using the same fluorescent membrane marker FM1-43, dye accumulation was observed at the SSC, around the nucleus and in the releasable vesicle pool (Harasztosi *et al.*, 2014). Cargo was also found to travel towards the apical pole of the cell. Application of FM1-43 to the basal pole resulted in transport in the basoapical direction; the transport speed was ~0.44 and ~0.08 μm/s at the distances of 5 and 67 μm, respectively, from the base of the cell (Harasztosi *et al.*, 2016). When applying the dye to both poles simultaneously, in order to compare the dynamics of the traffic in both directions, the apicobasal speed was about half the basoapical speed. However, the intracellular destinations of basally endocytosed vesicles, as well as the motor proteins involved in the transportation in the apicobasal and basoapical directions, have yet to be found.

1.5 Fluorescent markers

Fluorescent markers are an efficient tool for visualizing membrane recycling processes in living cells. In the present experiments, the fluorescent membrane markers FM1-43 and FM4-64 were used, as well as the fluorescent pinocytosis markers Lucifer Yellow and Dextran Oregon Green® 514, to visualize endocytosis in isolated OHCs.

1.5.1 Fluorescent membrane markers

FM1-43 is one of the most commonly used fluorescence markers for visualizing membrane uptake and transport in single cells; it has a maximum excitation/emission peak of 479/598 nm, respectively. It is an N-(3-Triethylammoniumpropyl)-4-(4(Dibutylamino) Styryl) Pyridinium Dibromide dye, that was first introduced as a marker of endocytic and exocytic processes at nerve terminals in frog (Betz & Bewick, 1992). This water-soluble dye is non-fluorescent in fluid, but it becomes intensely fluorescent when it binds rapidly and reversibly to the outer leaflet of the plasma membrane (Haugland, 2005) (Figure 7). Since vesicles are formed by using the plasma membrane, labelled vesicles can be detected and traced by fluorescent microscopy when they are transported in the cytosol. In OHCs it has been used in

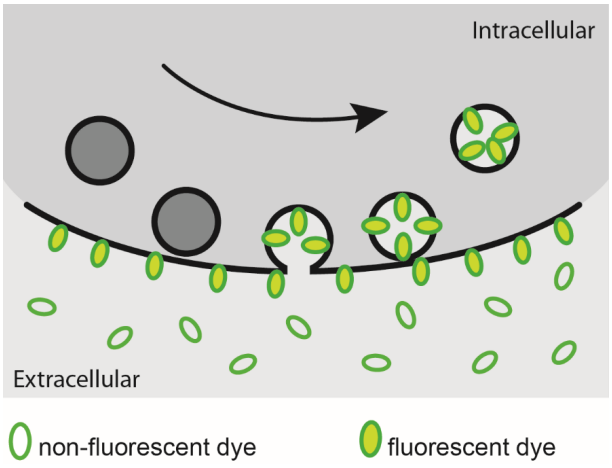

Figure 7. FM1-43/FM4-64 membrane labelling

Schematic diagram showing how FM1-43/FM4-64 stain the plasma membrane. These membrane markers are non-fluorescent in fluid, but fluoresce when bound to the plasma membrane. Therefore, they are appropriate for visualization of endocytosed vesicles and their intracellular trafficking, because as soon as they are endocytosed they reveal intracellular vesicle routes. / With kind permission from Dr. E. Harasztosi /

several studies to investigate endocytosis and transcytosis (Meyer *et al.*, 2001; Griesinger *et al.*, 2004; Kaneko *et al.*, 2006).

FM4-64 is a (N-(3-Triethylammoniumpropyl)-4-(6-(4-(Diethylamino) Phenyl) Hexatrienyl) Pyridinium Dibromide dye; it has a maximum excitation/emission at 506/750 nm, respectively. As a derivative of FM1-43 it has similar membrane labelling properties and is therefore also utilized as a marker for membrane uptake and transport in cells (Fischer-Parton *et al.*, 2000; Kutsuna & Hasezawa, 2002; Bolte *et al.*, 2004). This membrane marker is also fluorescent only when entering a lipophilic environment (Smith & Betz, 1996), e.g. the phospholipid membrane of the OHC. From there it is transported through endocytosis into the cell and towards different intracellular destinations (Figure 7). Like FM1-43, in OHCs it has been used to label hair cells (Meyers *et al.*, 2003). Having different excitation/emission wavelengths compared to FM1-43, it can be used for double-labelling experiments with FM1-43 (Harasztosi *et al.*, 2018).

1.5.2 Fluid-phase markers

Lucifer Yellow is a low molecular weight (MW = 521 Da) marker for fluid-phase with a maximum excitation/emission at 428/536 nm. It has been used as a marker for pinocytosis in neurons, epithelial cells and IHCs (Mundigl *et al.*, 1993; Mamdouh *et al.*, 1996; Griesinger *et al.*, 2002). When used at a concentration of 20 mM at the apical pole of OHCs, uptake was shown in the infracuticular tubular structures, which represent the early apical endosome (Griesinger *et al.*, 2004). The further intracellular distribution of the dye resembled that of the membrane marker FM1-43.

Dextran Oregon Green® 514 (MW = 10,000 Da) is a high molecular weight fluorescent dextran with an excitation/emission maximum at 496/524 nm. Dextrans are biologically inert hydrophilic polysaccharides used as a marker for pinocytosis or phagocytosis.

1.6 Confocal laser-scanning microscopy

Confocal laser-scanning microscopy techniques are widely used to visualize fluorescent organic or inorganic samples. These techniques differ from conventional light microscopy, in that in laser scanning microscopy the investigated object is scanned point-by-point with the laser and the emitted light intensity displayed as a function of position in order to reconstruct a visual image of the sample.

Single-photon confocal microscopy is a microscopic technique for acquiring high-resolution optical images of biological objects. One of its most important features is optical sectioning, the point-by-point detection of objects laying in a focal plane. This property allows the user, after the imaging process is completed, to reconstruct the acquired image in three dimensions. Of significant optical importance is the confocal blender, called pinhole, which is used as an aperture to limit the amount of incoming light from the object. The pinhole has a diameter of a few micrometres and can be variably adjusted so that it rejects the incoming light from the area outside of the focal plane. The size of the pinhole is measured in Airy units (AU). When set to higher values, the thickness of the focal plane is increased. If set to lower values, the thickness of the focal plane is decreased, and therefore the amount of detected light in the extrafocal space is decreased, leading to a more defined and contrasted image. Excessive reduction of the pinhole also decreases the intensity of the detected signal, which makes balancing the opening of the pinhole between the maximum and the minimum values a necessity.

Two-photon microscopy is a microscopic technique using a shorter excitation wavelength compared to the emission wavelength. Its key feature is that two photons occurring almost simultaneously (< 200 fs) are required to achieve the desired excitation state of a fluorescent molecule. This type of excitation allows high-resolution and high-sensitivity fluorescent microscopy in intact neural tissue (Svoboda & Yasuda, 2006). Two-photon fluorescent microscopy has several advantages to single-photon confocal microscopy: 1) reduced photobleaching and phototoxicity, together referred to as photodamage, 2) deeper penetration of the tissue (up to a few micrometres), 3) high-sensitivity imaging due to restricting the influence of the excitation light on the signal and, therefore, reducing scattering, and

4) photochemical reaction within a subfemtoliter volume can be initiated inside living cells and tissues (So *et al.*, 2000).

Figure 8 illustrates the differences between the two techniques. In this study, depending on contrasting experimental settings, both techniques were used. The quintessential difference between single-photon and two-photon microscopy is that, as the names suggest, a different numerical value is used in order to reach the excitation state of the molecule.

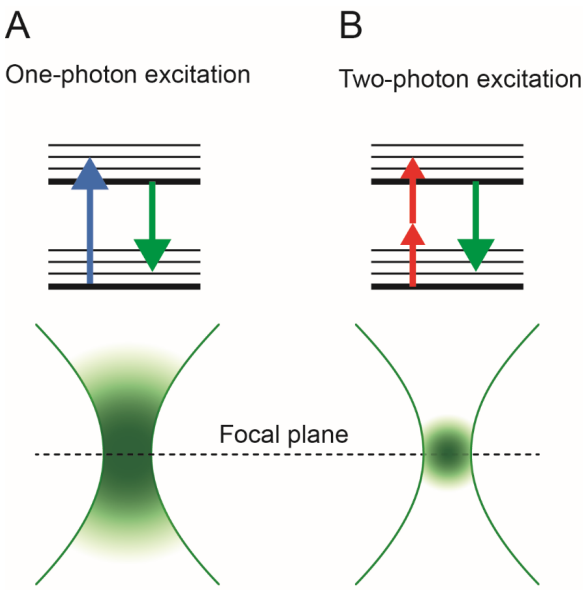

Figure 8. One-photon vs two-photon excitation

(A) In single-photon excitation, the energy of one photon is required to excite electrons of the dye molecule to a higher energy state. (B) In double-photon excitation, the energies of two photons are required at nearly the same time (< 200 fs) to excite the dye molecule, because the energy of a single photon is half the energy used for single-photon excitation. Because excitation occurs exclusively in the confocal plane for two-photon excitation there is almost no scatter from regions outside the focal plane; therefore, use of a pinhole is not required and most of the emitted light can be collected.

1.7 Aim of the study

The apical pole of the OHC has been the focus of endocytic research over the past years (Meyer *et al.*, 2001; Griesinger *et al.*, 2004; Kaneko *et al.*, 2006). Recently, basal endocytic activity was investigated (Harasztosi *et al.*, 2014) and the dynamics of basoapical vesicle traffic compared to that of apicobasal traffic (Harasztosi *et al.*, 2016). In order to be able to investigate apical and basal endocytosis by applying fluorescent dye solely to the desired location, a new perfusion system was developed (Harasztosi *et al.*, 2018) and applied in this study. It enables discrimination between apical and basal uptake by applying fluorescent dye exclusively to one pole of the cell. Using this perfusion system, the goal in the present study was to elaborate the different types of endocytosis and transcytosis mechanisms in the OHC.

In the case of endocytosis, the goal of this study was to clarify the processes involved in molecule internalization at each pole of the cell. Therefore, a blocker of pinocytosis and phagocytosis was applied as well as a blocker of clathrin-mediated endocytosis, and the apical and basal uptake of FM1-43 investigated. Furthermore, the effect of both blockers was compared to controls to elucidate how different types of endocytosis participate in apical and basal molecule internalization.

After clarifying which uptake mechanisms exist at the apex and base of the cell, another goal of this study was to quantify the molecular-weight limit of internalized cargo. The focus was on quantifying pinocytosis, since this type of uptake is known to be present at both the apex and base of the cell. Fluid-phase markers of different molecular weight were applied ubiquitously to the cell and possible uptake investigated.

In terms of transcytosis, the goal of the study was to compare the dynamics of apicobasal and basoapical traffic, to clarify the targets of basally endocytosed vesicles and to elucidate the pathways and motor proteins involved in traffic in both directions. To compare apicobasal and basoapical traffic, control experiments with solely apically labelled cells were conducted, to gather comparable data for the apex-to-base trafficking. While the intracellular destinations of apically endocytosed product are known, there is no data regarding the intracellular targets of basally endocytosed product. Therefore, OHCs were preincubated with an ER and mitochondria marker, to stain these structures, and FM4-64 applied basally to

visualize whether there is colocalization occurs between the structures labelled by the different dyes.

There is still no data available today to describe the significance of the different types of transport proteins in apicobasal and basoapical trafficking. Since it is known that there are mainly two different pathways in epithelial cells (Sec. 1.4.1.), the effect of blockers of the microtubular motor protein kinesin and the actin filament motor protein myosin VI was investigated. Traffic pathways in OHCs are not solely restricted to active transport along a longitudinal axis, but also from the centre towards the basolateral membrane. Hence, the influence on the blockers of the motor proteins to the SSC-traffic, as a lateral traffic, was further investigated and compared to the longitudinal traffic.

In summary, the goals of the study were to elucidate the endocytosis and transcytosis mechanisms in the OHC.

2 Materials and methods

2.1 Experimental animals

In this study 67 mature, healthy, pigmented or albino guinea pigs, with an approximate weight of 400-900 g, were used. “The study was approved by the Animal Protection, Veterinary Service and Veterinary Medicine Department of the University of Tübingen and by the Regional Council Tübingen (Reference number: 11.03.2014, 16.03.2015 complying with legal requirements of the European Communities Council Directive of 24 November 1986 (86/609/EEC)) for the protection of animals used for experimental purposes” (Harasztosi *et al.*, 2018). The animals derived from the breeding program of the Section of Physiological Acoustics and Communication, Department of Otolaryngology Tübingen (Einrichtung für Tierschutz, Tierärztlichen Dienst und Labortierkunde, directed by Dr. Franz Iglauer).

2.2 Isolation of OHCs

An already established isolation technique was used to extract OHCs from the cochlea (Preyer *et al.*, 1994). The experimental “animals were anesthetized by intraperitoneal injection of a mixture of 100 mg/kg ketamine and 4 mg/kg xylazine and were killed by rapid cervical dislocation” (Harasztosi *et al.*, 2018). “Temporal bones were dissected from the skull and placed in ice-chilled Hanks’ balanced salt solution (HBSS, Biochrom GmbH, Berlin, Germany)” (Harasztosi *et al.*, 2018). A physiological salt solution was used as a basic extracellular solution throughout the experiments: (in mM): NaCl, 137; KCl, 5.4; $CaCl_2$, 1.25; $NaHCO_3$, 4.2; $MgSO_4 \cdot 7H_2O$, 0.81; KH_2PO_4, 0.35; Na_2HPO_4, 0.34; D-glucose, 5.0 and HEPES, 5. The osmolarity of this extracellular solution was set to 310 mOsm/L and the pH to 7.25 using D-glucose and NaOH. The correct numerical value of the osmolarity and the pH were controlled with an osmometer (Osmomat 030, Gonotec GmbH, Berlin, Germany) and pH-meter (Microprocessor pH Meter, Hanna Instruments, Vöhringen, Germany), respectively. The wall of the middle-ear cavity was partially removed to access the

cochlea. The bony wall of the cochlea was opened with a scalpel in HBSS under a preparation stereomicroscope (Leica MS5, Leica Mikrosysteme Vertrieb GmbH, Wetzlar, Germany) to expose the modiolus and the organ of Corti. Stripes of the organ of Corti were carefully separated from the modiolus using a fine needle and placed for 10 minutes into 200 µL HBSS containing collagenase-IV enzyme from *Clostridium histolyticum* (1 mg/mL, Sigma-Aldrich Chemie GmbH, Munich, Germany). The enzymatic treatment served primarily to enhance the cell isolation process, and also to free the basal pole of the OHC of most of the nerve endings. After the enzymatic treatment, OHCs were isolated by mechanical dissociation using a 100 µL Eppendorf pipette. Cells were allowed 10 minutes to settle down and adhere to a poly-L-lysine (Cell-Tak™, Corning Inc., Corning, NY, USA) coated coverslip in 200 µL HBSS. The filling of the chamber was conducted with ~2 mL HBSS with or without the utilized blocker in the case of endocytosis and transcytosis blocking experiments.

Two criteria were used to choose appropriate cells for experiments: 1) intact cells possessing a typical cylindrical cell body without intracellular Brownian motion, and 2) cells without obvious damage to the hair bundle. In the following experiments, only cells which met these criteria were included in the study (n = 120), where the cell lengths were in the range from 50 - 86 µm. “All experiments were conducted at a controlled room temperature of 21.5 ± 0.5 ºC” (Harasztosi *et al.*, 2018).

2.3 Fluorescent markers

To visualize endocytosis, the fluorescent membrane markers FM1-43 and FM4-64 were used. All fluorescence markers were purchased from Thermo Fisher Scientific, Inc. (Waltham, MA, USA). Both are amphiphilic probes that partition with lipid bilayers but do not cross them and have similar membrane labelling properties, but FM4-64 is distinguishable in that it exhibits long-wavelength red fluorescence compared to the spectra of FM1-43. In both cases, stock solutions in the concentration of 10 mM were prepared in dimethylsulphoxide (DMSO). Both dyes were used at the final concentration of 10 µM. In all cases, the fluorescence markers were diluted to the final concentration in HBSS on the day of use.

To visualize pinocytosis, the fluorescent fluid-phase markers Lucifer Yellow and Dextran Oregon Green® 514 were used. For Lucifer Yellow, a stock solution in the concentration of 50 mM was prepared in DMSO. The final concentration for Lucifer Yellow was 50 µM. For Dextran Oregon Green® 514, a stock solution in the concentration of 2.5 mM was prepared in DMSO. The final concentration for Dextran Oregon Green® 514 was 10 µM.

To visualize the colocalization of basally endocytosed vesicles and the endoplasmic reticulum (ER), the membrane marker FM4-64 and the fluorescent ER-marker $DiOC_6$ were used. To label the ER, cells were incubated in the fluorescent endoplasmic marker $DiOC_6$ (Terasaki, 1989). A stock solution of 1 mg/mL was prepared for $DiOC_6$ in DMSO; just before the experiments, it was diluted with HBSS at a final concentration of 0.87 µM (Kaneko *et al.*, 2006). The 1-minute-long incubation step was included after enzymatic treatment.

2.4 Endocytosis and intracellular traffic blockers

The inhibition of endocytosis as well as the inhibition of motor proteins was investigated.

In the first set of uptake-blocker experiments, OHCs were preincubated with phenylarsine oxide (PAO), a blocker of pinocytosis and phagocytosis (Dutta & Donaldson, 2012), and the apical and basal uptake of FM1-43 was tested. Stock solution of PAO in the concentration of 40 mM was prepared in DMSO. Isolated cells were preincubated with PAO for 30 min using the final concentration of 80 µM. Stock solution of the CME-associated blocker concanavalin A (ConA) (Dutta & Donaldson, 2012) in the concentration of 50 mM was prepared in phosphate buffered saline (PBS). Cells were preincubated for 30 minutes with ConA using the final concentration of 50 µM to test the apical and basal uptake of FM1-43. For both the PAO and the ConA blockers, the incubation step was started after the isolated cells had settled onto the cover slip. The incubation process meant that the experimental chamber was loaded up to 2 mL with HBSS containing the blockers via an Ismatec high-precision multichannel dispenser (IDEX Health & Science GmbH, Wertheim,

Germany). The perfusion rate was set to a slow perfusion rate of 14 µL/min in order not to disturb cell adhesion.

As a second set of experiments, the involvement of motor proteins for the intracellular traffic was investigated by blocking them independently. For inhibition of kinesin, the motor protein responsible for traffic towards the minus end of the microtubules, the blocker monastrol (Griesinger *et al.*, 2004) was used. Cells were preincubated with this kinesin blocker for 30 minutes. A stock solution of 50 mM was prepared for monastrol in DMSO. The final concentration of monastrol was 25 µM. Both the apicobasal and the basoapical FM1-43 trafficking were investigated. To block myosin VI, cells were incubated in 2,4,6-Triiodophenol (TIP) an efficient blocker of that motor protein (Bond *et al.*, 2013), for 30 minutes. A stock solution of 25 mM was prepared for TIP in DMSO. The final concentration for TIP was 40 µM. Similarly to the previous experiments, both the apicobasal and the basoapical traffic were investigated. As in the case of blockers of endocytic activity, for both blockers the incubation step of the protocol was started after the cells had settled for 10 minutes onto the coverslip. For that process, the experimental chamber was loaded up to 2 mL with HBSS containing the blockers using the Ismatec high-precision multichannel dispenser. All blockers were purchased from Sigma-Aldrich (Sigma-Aldrich Chemie GmbH Munich, Germany).

In the uptake-blocker and the traffic-blocker experiments, the drugs were not washed out from the experimental chamber before beginning the fluorescence measurements.

2.5 Perfusion systems

Two different perfusion systems were used to apply fluorescence markers to the isolated OHCs for investigating endocytic activity and intracellular transport. In the case of general endocytosis investigation, a single-barrel (multichannel) perfusion system was used, whereas for separating molecule internalization either apically or basally, the newly-developed double-barrel perfusion system was used (Harasztosi *et al.*, 2018). Despite being used for different purposes, the two perfusion systems had several aspects in common:

- In both cases, a perfusor was constructed as either a single-barrel or a double-barrel system." For connecting the perfusor barrel to the perfusion pump, an Eppendorf GELoader® (Eppendorf Vertrieb Deutschland GmbH, Wesseling-Berzdorf, Germany) was inserted into a barrel with its exit close to the shank and fixed in place with silicone glue (RAU-SIK Adhesive SI 1511, Raumedic, Helmbrechts, Germany) injected into the barrel, using a 1-mL insulin syringe and needle (size: 27 G 3/4", 0.4 x 19 mm^2)". (Harasztosi *et al.*, 2018) The silicon glue was pushed as close as possible to the end of the Eppendorf GELoader® tips. Because of the relatively long curing time, the perfusor was prepared at the latest by the day before the experiment.
- The perfusors were positioned near the cell using a micromanipulator (Luigs and Neumann SM5, Luigs and Neumann GmbH, Ratingen, Germany)." For connecting to the micromanipulator, the perfusor was fixed to a metal rod with a length of ~15 cm and diameter of ~3 mm, using a cold-curing resin (Technovit® 3040, Heraeus Kulzer GmbH Division Technik, Wehrheim, Germany)". (Harasztosi *et al.*, 2018)
- "The perfusant was driven by a four-channel Ismatec perfusion pump (IDEX Health & Science GmbH, Wertheim, Germany)". (Harasztosi *et al.*, 2018)
  The flowrate was set to maintain laminar fluid flow around the cell.

2.5.1 Single-barrel perfusion

"To establish homogeneous plasma-membrane labelling, fluorescent dye was applied through a single-barrel perfusion system. The perfusor tip had an inner diameter of ~350 µm and was positioned ~450 µm from the cell" (Harasztosi *et al.*, 2018). The perfusor was constructed from an Eppendorf epT.I.P.S.® pipette tip (standard, 0.5 – 20 µL), into which two Eppendorf GELoader® tubes were glued for connection to the perfusion pump. The flow rate was set to 14 µL/min to achieve laminar flow." For dye application, the perfusion system was switched from dye-free to dye-loaded extracellular solution by manually switching the solutions via three-way stopcocks which were built into each channel". (Harasztosi *et al.*, 2018)

The advantage of this single-barrel perfusion system is that it enables the plasma membrane to be stained homogeneously, therefore allowing simultaneous plasma-membrane labelling of the apical and the basal poles of isolated cells.

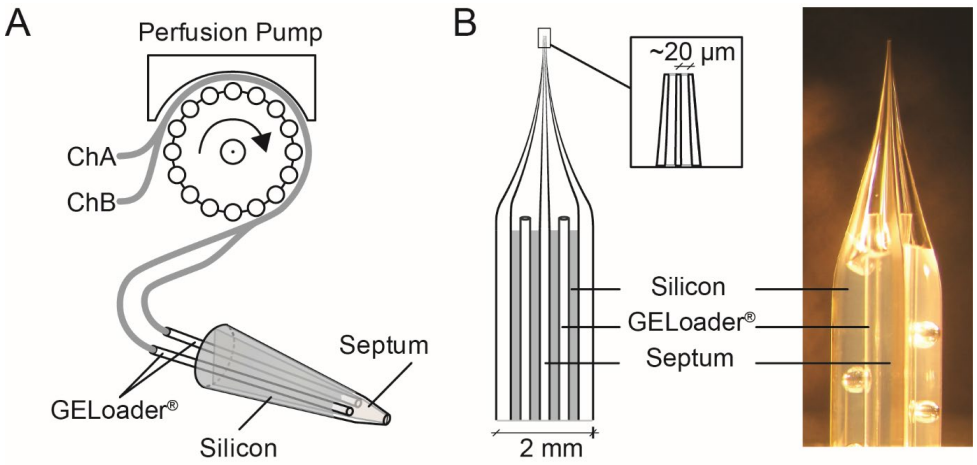

Figure 9. Double-barrel perfusor

(A) Schematic drawing illustrating the construction of the double-barrel perfusion system. The dye is driven by a perfusion pump by two channels (ChA and ChB). Glass capillary in theta style are used to fabricate the double-barrel perfusor. An Eppendorf GELoader® tube is fixed into each barrel of the capillary using silicon glue (dark grey region). The glass capillary has a septum which separates both barrels from each other (light grey region). The silicone was loaded almost up to the opening of the GELoader® tips. (B) Schematic drawing and a picture of a prepared perfusor tip. (left) At the tip, the distance from the septum to the inner wall of the barrel is ~20 µm. The outer diameter of the glass capillary is 2 mm. (right) Air bubbles occurring during the silicone-glue filling process can be seen in the capillary. Figure from Harasztosi *et al.* (2018)

2.5.2 Double-barrel perfusion

"To allow independent staining of the apical and basal poles, either separately or concurrently, a double-barrel perfusion system was developed in our lab" (Figure 9) (Harasztosi *et al.*, 2018)." A double-barrel, premium standard wall borosilicate-glass, theta capillary with an external diameter of 2 mm (Harvard Apparatus, MA, USA) was pulled with a DMZ-Universal Puller (Zeitz Instruments, Augsburg, Germany)". (Harasztosi *et al.*, 2018). "At the tip of the perfusor, the distance between the septum and the inner wall of the barrel was ~20 µm". (Harasztosi et al., 2018) "Contrary to the situation for the single-barrel perfusor, it was necessary to place the perfusor tip as close as possible to the cell to ensure localized application". (Harasztosi et al., 2018). The distance to the OHC was ~30 µm. Given this relatively short distance and the relatively high pressure produced by the small lumen of this type of barrel tip, two additional precautions, not required for the single-barrel

perfusor, were necessary to ensure that the cell remained fixed to the coverslip: 1) the poly-L-lysine coated coverslip was additionally coated with the cell-and-tissue adhesive Cell-Tak™ (Corning Inc., Corning, NY, USA), and 2) the flow rate was set as low as possible (3 µL/min per barrel).

The laminar fluid flow established by this double-barrel perfusor (Figure 10) supports the following type of experiment: Application of a single dye to either the basal or the apical half of the cell when dye-free HBSS is pumped into one barrel and dye containing HBSS into the other barrel. The advantage of this double-barrel perfusion system is that the dye-free fluid application from one barrel has a “shielding” role, enabling dye to be applied from the other barrel exclusively to one pole of the cell protecting from diffusing to the other pole.

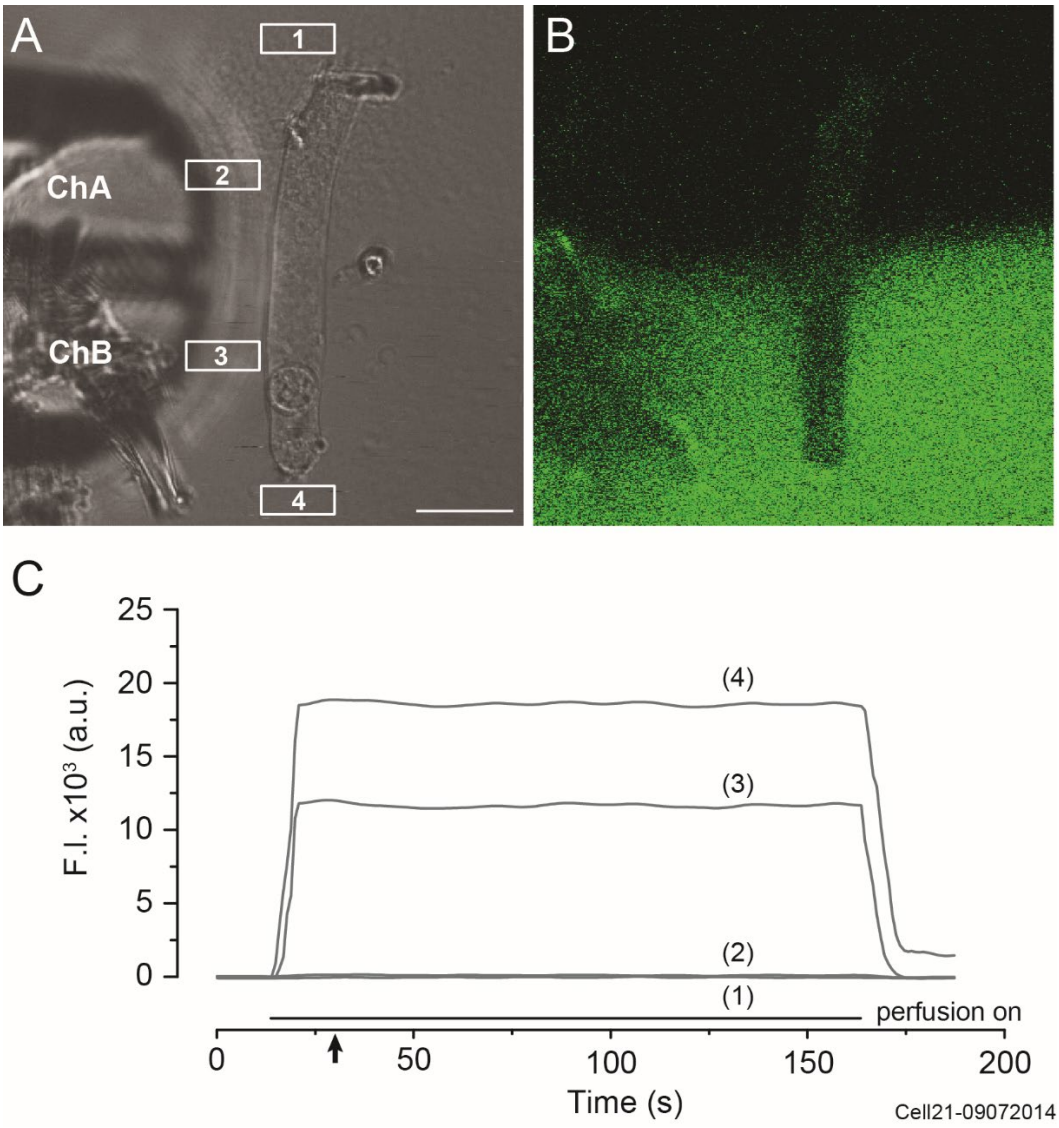

Figure 10. Laminar fluid flow

(A) DIC image showing the experimental configuration. A double-barrel capillary is positioned close to an OHC to establish a double-stream laminar fluid flow. The upper barrel (ChA) of the capillary is filled with dye-free HBSS and the lower barrel (ChB) with HBSS containing 50 μM fluo-3, a fluorescent calcium indicator. (B) The fluorescent image demonstrates the result of double-steam laminar fluid flow established by the double-barrel perfusion. Namely, the fluorescence is restricted to the fluid around the basal half of the cell, indicating no obvious dye diffusion into the region around the apical half of the cell where the dye-free fluid was applied. (C) Fluorescence signal-intensity values derived from the numbered ROIs in panel A. The arrow indicates the recording instant of the image in panel B. The fluorescence intensities in ROIs 3 and 4 were elevated and time invariant during the perfusion. The signals in ROIs 1 and 2 were no different to background noise, indicating the protective role of the dye-free solution applied from ChA. Cell length, 83 μm. Scale bar, 20 μm. /Data and figure with the kind permission from Dr. C. Harasztosi/.

2.6 Confocal laser scanning microscopy

Fluorescence signals were recorded using a Zeiss Axioskop2 FS mot microscope (Zeiss, Heidelberg, Germany) equipped with a Zeiss LSM 510 confocal system and with a two-photon laser system (Mira^{TM} 900 Ti:Sapphire Laser pumped by a Verdi V5 Diode-Pumped Laser from Coherent, Santa Clara, USA). In the case of single-photon excitation, the pinhole diameter was set to 1 AU corresponding to a section thickness of 2.4 µm, using a Zeiss 40x IR-Achroplan water-immersion objective with NA 0.8. For data acquisition, Zeiss ZEN2009 software was used. Images were recorded in 1024 x 1024 pixel² resolution; the voxel size was ~0.3 x 0.3 x 2.4 µm^3.

In the case of FM1-43 labelling, the dye was excited with an Argon laser (λ_{ex} = 488 nm) with a laser power of 1% and the emitted light was recorded above 505 nm. In the case of FM4-64 labelling, the dye was excited with a HeNe laser (λ_{ex} = 543 nm) with a laser power of 1% and the emitted light was collected with a LP505 longpass filter. In the case of preincubation with $DIOC_6$ and basal labelling with FM4-64, the dyes were excited with the argon laser (λ_{ex} = 488 nm) with a laser power of 1% and the emitted light was collected in two channels. For Channel 1, the $DiOC_6$ emitted light was recorded using a BP500-550 bandpass filter and for Channel 2 the FM4-64 emitted light was recorded using a BP 650-710 bandpass filter.

In the case of the fluid phase markers Dextran Oregon Green® 514 and Lucifer Yellow, the two-photon laser excitation was chosen for imaging to avoid background noise from scattering outside the focal plane which would have been present for single-photon excitation (Sec. 1.6.). Therefore, on application of Lucifer Yellow, the dye was excited with the two-photon laser (λ_{ex} = 840 nm) with a laser power of 15% and the emitted light collected using a KP650 shortpass filter. The Dextran Oregon Green® 514 was excited with the same laser and emitted light collected using the KP650 shortpass filter.

2.7 Electrophysiology

OHCs were whole-cell voltage clamped to investigate a possible intracellular-potential effect on the fluorescence dye uptake.” For this purpose, patch pipettes were fabricated with a P-87 Flaming/Brown type micropipette puller (Sutter Instrument Company, Novato, U.S.A.), using soda-glass capillaries (Hildenberg GmbH, Malsfeld, Germany) and connected to an EPC-9 patch-clamp amplifier (Heka Elektronik, Lambrecht, Germany)”. (Harasztosi et al., 2016) “Pipettes were filled with (intracellular) solution containing (in mM): 135 CsCl, 10 HEPES, 2 $MgCl_2$, 0.1 CaCl2, 11 EGTA (pH 7.2, osmolarity 320 mOsm/L)”. (Harasztosi et al., 2016). The pipette resistance, measured in the (extracellular) bath solution, was 1.5–2 MΩ. Series resistance was reduced by at least 60% by compensation online. After the whole-cell configuration was established, the optical data acquisition process was started. During the extracellular dye application phase, the membrane potential of the cell was rapidly changed from the holding potential of -60 mV to 0 mV and the influence of depolarization on the intracellular labelling was investigated.

2.8 Data analysis

In order to quantify the fluorescence light intensity in different areas in the focal plane, the Region of interest (ROI) function of the ZEN 2009 software was used. This option allows the user to measure the fluorescence intensity as a function of time in a given area. To normalize fluorescence intensity values, similar size of ROIs were selected and placed at a similar distance from each other and from the plasma membrane of the cell. Another ROI was placed in the extracellular environment to measure the background signal outside of the cell. The background fluorescence signal was subtracted from the measured values in each intracellular ROIs. The distances from each ROI to the apical/basal plasma membrane as well as the total cell length were measured in µm using the ZEN software.

In the case of colocalization experiments of $DiOC_6$ with FM4-64, the colocalization function of the ZEN 2009 software was used. This function allows analysis of a two-channel image for fluorescence colocalization by plotting every pixel of an image in a diagram based on its intensity level from each channel. Furthermore, a 3D view function of the software was used to render a Z-stack image (in 1 µm steps) as a three-dimensional object. This mode helped in the analysis to reveal both the single- and the double-labelled structures.

In the SSC-traffic experiments, ROIs were placed in the SSC area where plasma-membrane staining was absent, in order to avoid the plasma membrane influencing the fluorescence intensity. For comparison of the speed to reach a certain fluorescence intensity in the SSC, similar size ROIs was placed at the corresponding distance.

Data were analysed offline using Microsoft Excel (Microsoft Corporation, Redmond, WA, USA) and Origin 7.0 (OriginLab Corporation, Northhampton, MA, USA). To determine the fluorescence signal delay to the plasma-membrane signal, a threshold was set as 20% of the plasma-membrane signal-saturation level.

Data are presented as average and standard deviation (SD). Differences between averaged data were evaluated with the Student's *t*-test and were considered significant if $p < 0.05$. The test value is given as t_f where f is the degree of freedom. "Data were fitted either with linear regression or with a single exponential function using the Levenberg–Marquardt algorithm in Origin7". (Harasztosi et al., 2016).

3 Results

3.1 Uptake and trafficking

In the first set of experiments, either FM1-43 or FM4-64 fluorescent membrane markers were applied to the apex of the cell, in order to investigate the time dependency of intracellular labelling (Figure 11). This apicobasal data will be compared with data gained in the previous study, where the basoapical traffic was investigated (Harasztosi *et al.*, 2016). In that study, the speed of the apicobasal

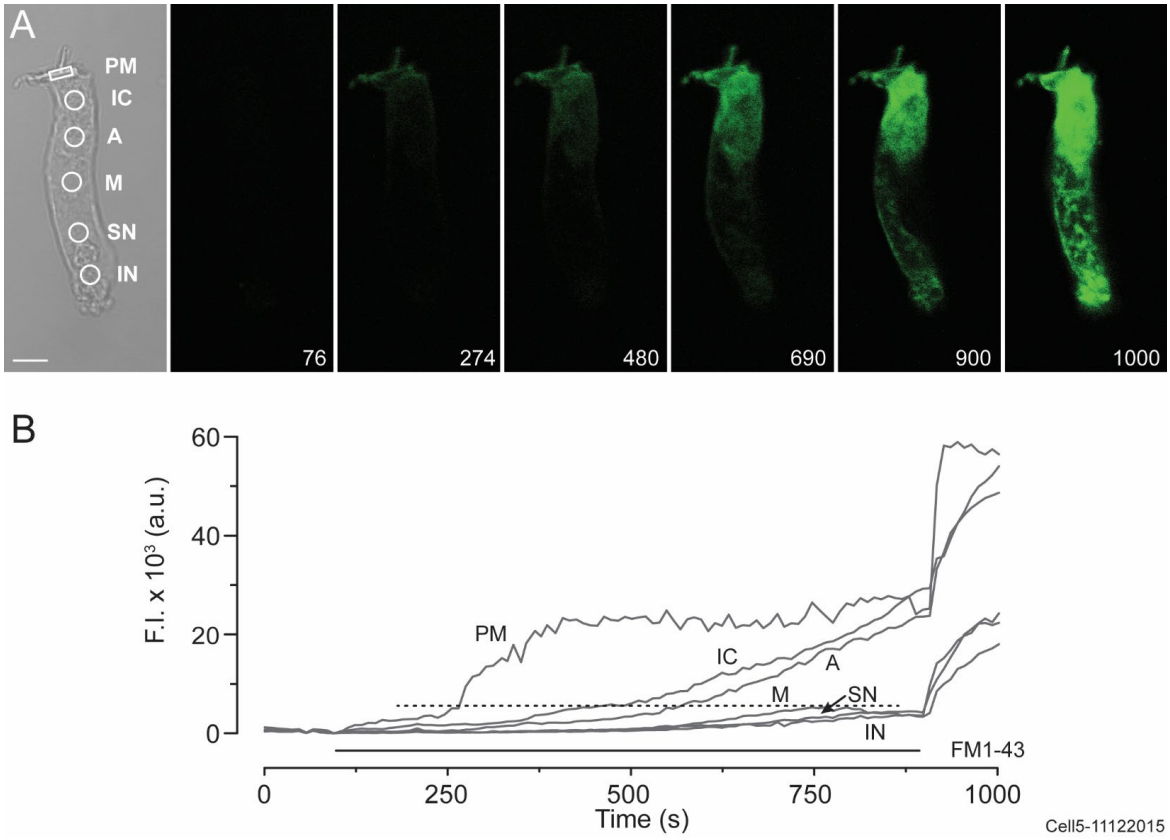

Figure 11. FM1-43 apical staining of the isolated OHC

(A) DIC image demonstrating the location of ROIs. Plasma membrane (PM), infracuticular (IC), apical (A), middle (M), supranuclear (SN) and infranuclear (IN) areas. The fluorescence images demonstrate FM1-43 uptake in time. Numbers in the bottom right corner of the images indicate the experimental time. (B) Fluorescence intensity (F.I.) measured in the given ROIs in time. At the beginning of dye application FI rapidly increases in the PM and increases more slowly in the other ROIs. Dashed line indicates the set 20% threshold for further data analysis. Scale bar, 10µm.

traffic was determined in cells which were double labelled when membrane “markers were applied to both the apical and the basal poles of the OHC”. (Harasztosi et al., 2018). To ensure that dye interaction did not influence the observations, data for solely apically labelled cells were acquired in the present study. Thereby it is possible to make appropriate comparisons of the uptake and traffic.

Therefore, in the first set of experiments single labelled OHCs (n = 5) were used; the cell length was 68 ± 8 µm. The membrane marker was applied exclusively to the apex of the cell using the double-barrel perfusion system (Sec. 2.5.2) and fluorescence intensity changes were observed with a confocal laser scanning microscope at a resolution of 1024 x 1024 pixels/frame. In the example in Figure 11, the fluorescence labelling was recorded for 15 minutes with a scan interval of 5 sec and a scan time of 1.97 sec. The fluorescence intensity was measured in different regions of the cells. For this purpose, for each cell, five similar sized circular ROIs were placed at the infranuclear (IN), apical (A), middle (M), supranuclear (SN) and infranuclear (IN) areas of the cell. Furthermore, one ROI was placed at the apical plasma membrane to measure the plasma-membrane staining at the apex of the cell (Figure 11A). The fluorescence pictures show that the fluorescence intensity starts to increase first in the plasma membrane region at the apex of the cell, but later it also increases in the intracellular regions, indicating dye uptake (Figure 11B). The progress of the intracellular labelling towards the base of the cell implies labelled vesicle traffic towards the basal pole.

To compare the dynamics of dye uptake at the apical (present experiments) and basal (Harasztosi *et al.*, 2016) poles, the time delay relative to the plasma membrane was calculated, respectively, in the infracuticular and infranuclear ROIs. The time delays are 50 ± 23 s (n = 5) and 14 ± 5 s (n = 7) in the infracuticular and infranuclear ROIs, respectively. These values are significantly different (t_{10} = 4.49, p = 1.16 * 10^{-3}), “implying that the endocytic activity at the basal pole of the OHC is more intense compared to the apical pole”. (Harasztosi et al., 2014).

To compare the dynamics of apicobasal (n = 5; present study) and basoapical (n = 7; (Harasztosi *et al.*, 2016)) vesicle traffic, onset time delays were determined for all the ROIs along the OHC. The data are presented in Figure 12 as distance as a function of delay. The average data were fitted using linear regression with the axis-intercept set to zero. The slope parameter is 0.129 ± 0.007 µm/s and 0.196 ± 0.015 µm/s for the apicobasal and basoapical signals, respectively. These values are

significantly different (t_8 = 8.15, p = 3.82 * 10^{-5}), indicating that the speeds of the traffic in the opposite directions are different, namely that towards the apex it is faster than towards the base of the OHC.

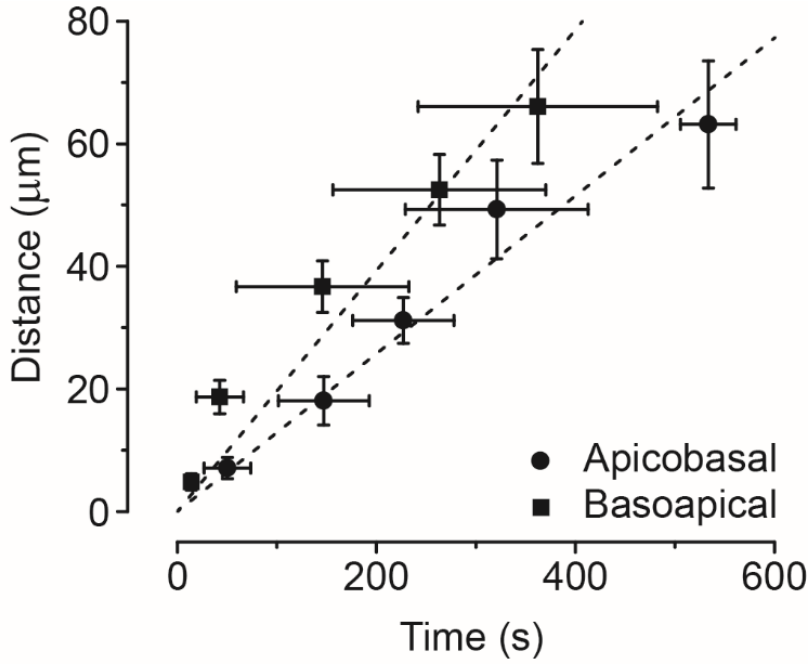

Figure 12. Apicobasal vs basoapical traffic

The time-distance data demonstrate the delay of the fluorescence signals to reach the threshold in the ROIs relative to the plasma membrane signal. Circles demonstrate the values measured for the apical-uptake cells (present study) while squares show data solely from basal-uptake cells (Harasztosi *et al.*, 2016). Dashed lines are results of the linear regression of the average data in which the intercept was set to zero. The slope parameter is 0.129 ± 0.007 µm/s and 0.196 ± 0.015 µm/s for the apicobasal and basoapical signals, respectively. Note that the slope of the basoapical-traffic curve is significantly larger implying faster traffic towards the apex.

3.2 Quantification of MW-uptake limit

In the second set of experiments, uptake of fluid-phase markers with different molecular weight was investigated. For this purpose, dyes were applied through the single-barrel perfusion system ubiquitously to the extracellular fluid of the isolated OHC (Sec. 2.5.1).

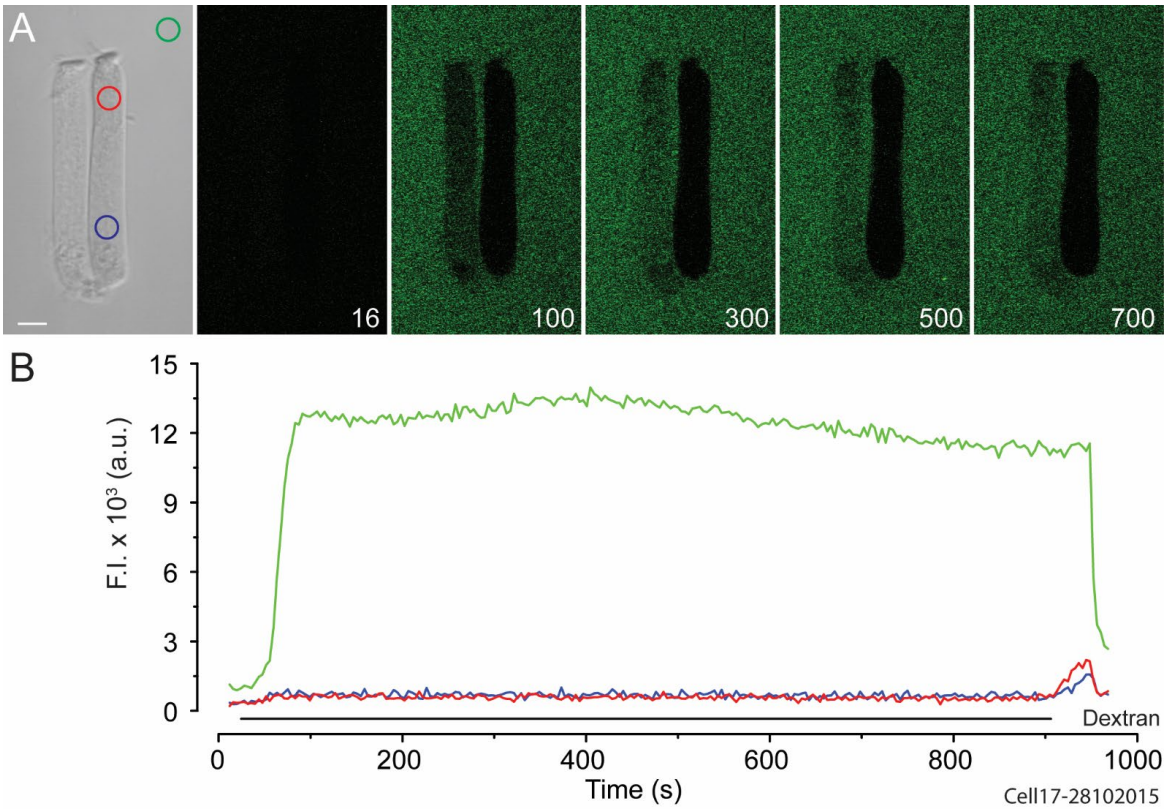

Figure 13. Dextran Oregon Green® 514 application

(A) DIC image shows OHCs and the locations of the ROIs used for analysis. The extracellular fluorescence signal was evaluated in the green circular ROI; the blue and the red ROIs were set for basal and apical intracellular regions, respectively. Fluorescence images show that although the dye was present extracellularly, there was no intracellular increase of the signal. Note that measurements are focussed on the cell on the right-hand side of the picture, because the other cell was out of the focal plane. (B) Fluorescence intensity values demonstrate the time dependence of the signals measured in the ROIs. Note that the extracellular intensity increases immediately after dye application (green solid line) and decreases after terminating the dye perfusion (black solid line). These observations imply that Dextran Oregon Green® 514 was not endocytosed. Apical and basal increases after terminating the dye application were related to an obvious movement artefact. Scale bar, 10µm.

In the first experimental configuration, the single-photon confocal system was used with the argon laser (λ_{ex} = 488 nm) to excite the high molecular-weight dye Dextran Oregon Green® 514 (MW = 10,000 Da, data not shown). This experimental configuration was not suitable for determining possible uptake of the fluorescence marker due to the detection of scattered light, which originated from the single-

photon excited dye molecules located in the extracellular fluid, outside of the confocal plane. It was concluded that due to the properties of the single-photon laser, which excites dye molecules located not only in the focal plane but also in the extrafocal space (Sec. 2.6), this type of excitation mode was not suitable for these experiments. Therefore, the two-photon laser, which excites dye molecules only in the confocal plane, was used. Thereby, it was possible to investigate intracellular fluorescence signal levels without the influence of fluorescence signals originating from extracellularly located dye. ROIs were placed intracellularly: at the basal pole (blue circle) and at the apical pole (red circle) (Figure 13A). A ROI (green) was placed in the extracellular environment. Staining was observed for 15 minutes at a resolution of 1024 x 1024 pixels/frame with a scan time of 1.97 sec. and a scan time interval of 5 sec. During the dye application, indicated by a black solid line, there was no significant increase of the intracellular signal, whereas a large signal was detected extracellularly (Figure 13B). This result shows that OHCs cannot endocytose molecules having molecular weight of 10,000 Da or higher.

To find a possible upper limit of molecular weight that OHCs can pinocytose, in the second experimental configuration the low molecular-weight Lucifer Yellow (MW = 521 Da) was applied through the single-barrel perfusor to the extracellular environment of the isolated OHC (Figure 14). During dye application, indicated by a black solid line, there was no increase in the intracellular signals, but there was stable and high fluorescence extracellularly (Figure 14B). This result indicates that,

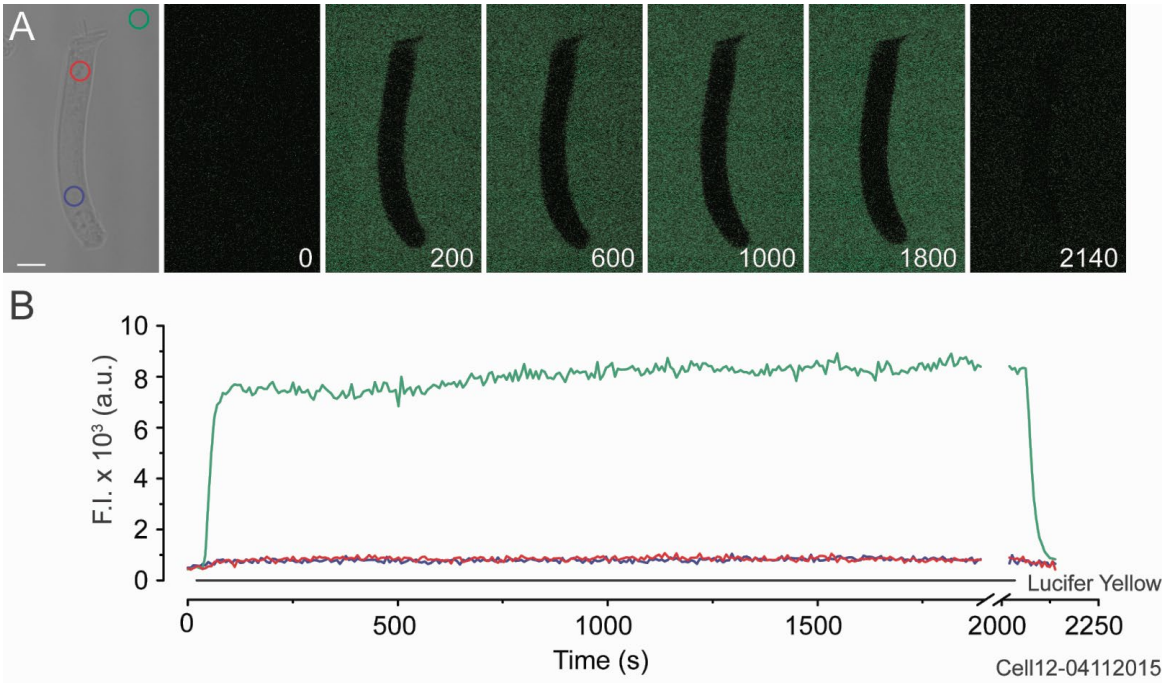

Figure 14. Lucifer Yellow application

(A) DIC image showing the placement of the different ROIs as in Fig. 13. The images show that there was no intracellular uptake (≤30 min.). (B) Fluorescence intensity (FI) as a function of time for each ROI. Note that there is no FI increase intracellularly. After terminating the dye application (solid black line), FI decreases extracellularly (green solid line). The time period of ~10 sec. with no FI signal around 2000 sec. due to the brief interruption of application to investigate a possible washout. Scale bar, 10 µm.

as in the case of Dextran Oregon Green® 514, there was no dye uptake, implying that molecules with molecular weight around 500 Da cannot be endocytosed by the OHC.

Lucifer Yellow and Dextran Oregon Green® 514 are both anionic molecules. To investigate whether the negative charges had an influence on the dye uptake, a series of control experiments were conducted by changing the transmembrane potential using the patch-clamp technique. As in the previous set of experiments, the extracellular environment of the cells was perfused with Lucifer Yellow (data not

shown). In these experiments, OHCs were depolarized from the holding potential of -60 mV to 0 mV for 30 s (n = 3) and for 100 s (n = 1). In that time interval, there was no detectable intracellular fluorescence signal. The measured relative fluorescence intensity change was $6.5*10^{-2} \pm 0.09$ (n = 4), which is not significantly different from zero (t_3 = 1.46, P_1 = 0.12). This result shows that Lucifer Yellow is not internalized and that depolarization does not facilitate Lucifer Yellow uptake. Therefore, the negative charge of the dye is not responsible for the absence of uptake.

These data, together with the previous molecular-weight experiments, imply that OHCs are not able to pinocytose molecules with a molecular weight larger than 500 Da. However, the data cannot rule out the possibility that molecules larger than 500 Da could be taken up by other types of internalization, such as clathrin-mediated endocytosis.

3.3 Intracellular targets of basally endocytosed vesicles

In these set of experiments, the intracellular destinations of a basally applied fluorescent membrane marker were investigated. First, the endoplasmic reticulum system of OHCs was labelled by $DiOC_6$ (Sec. 2.3) and then FM4-64 was applied. The advantage of using FM4-64 and not FM1-43 was that the fluorescence spectra of FM4-64 and $DiOC_6$ could be easily separated using filter sets. The fluorescent membrane marker was applied via the double-barrel perfusor exclusively to the base of isolated OHCs (n = 6) and the fluorescence signal collected at a resolution of 1024 x 1024 pixels/frame. The scan time was 6 min 30 sec with a reduced scan interval of 10 sec due to the known phototoxicity of $DiOC_6$, in order to reduce dye bleaching. One example cell was chosen to demonstrate the colocalization in time (Figure 15). Since the fluorescence signals were collected in two channels, the first scan was conducted to detect the $DiOC_6$ labelling. During the second scan, the FM4-64 dye propagation was recorded. The $DiOC_6$ labelling is demonstrated in Figure 15A, while the time dependency of the FM4-64 in Figure 15B. Figure 15C shows the merged image of Figure 15A and the last image of Figure 15B to demonstrate the colocalization of the two different dyes. This is represented by the yellow colouring of the overlapping intracellular spots, contrary to the prior clearly red and green

coloured dye localizations. This colocalization indicates that basally endocytosed FM4-64 travels to the previously labelled $DiOC_6$ destinations, namely ER and mitochondria systems of the OHC.

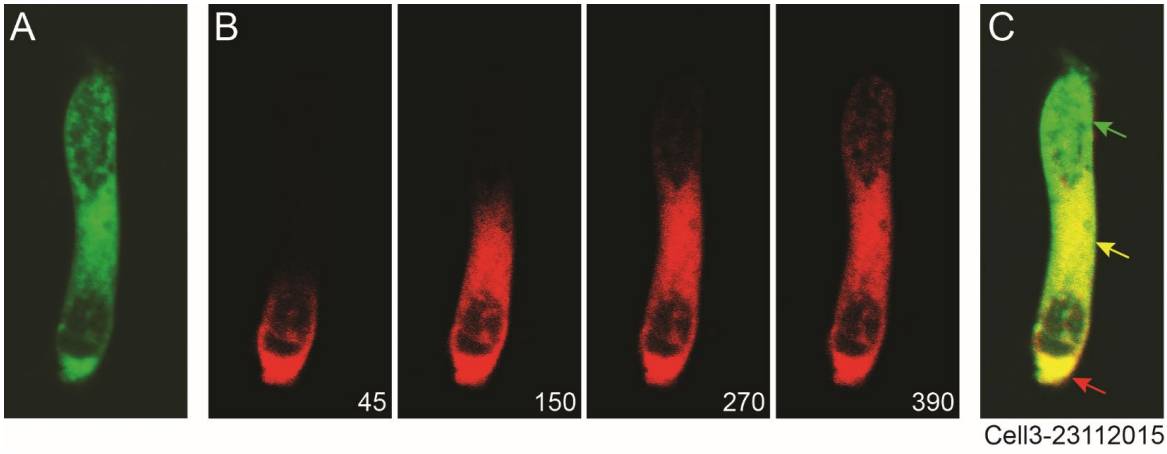

Figure 15. Colocalization

(A) The $DiOC_6$ labelled OHC. ER and mitochondria are stained. (B) FM4-64 visualizes basoapical vesicle traffic. Numbers indicate the experimental time in seconds. (C) Merged image of panel A and the last image of panel B. Note that beside the only red or green labelled areas, depicted by the red and green arrows, the colocalized structures, shown in yellow, are visible in the infranuclear pole and in the centre of the OHC up to the apical area (yellow arrow).

3.4 Endocytosis blockers

In these sets of experiments, to reveal the presence of different types of endocytic activities at both poles of the OHC, endocytic activity blockers were applied and signal delays were compared with data measured in untreated cells. To test the effect of different drugs on the dye uptake, OHCs were incubated for 30 min before the initiation of the fluorescence measurements either with concanavalin A (ConA), to block clathrin-mediated endocytic activity, or with phenylarsine oxide (PAO) to block pinocytosis and phagocytosis. Drugs were not washed out from the experimental chamber and were present during the fluorescence measurements. FM1-43 was applied either to the apical or to the basal pole. The intensity values were collected at a 1024 x 1024 pixels/frame resolution with a scan time of 10 min and scan interval of 5 sec. FM1-43-signal delays in the infracuticular and infranuclear regions to the plasma membrane labelling were measured. For determination of the dynamics of dye uptake either an infracuticular or an infranuclear ROI was chosen. The time delays in the infracuticular and the infranuclear regions for treated and untreated cells are summarized in Figure 16.

At the apex of the cell, both blockers caused a delay of the dye uptake (Figure 16A). The treatment either with ConA or PAO significantly increased the time delay compared to the control value of 50 ± 23 s to 125 ± 55 s (t_{11} = 3.23, p = 0.008) and to 156 ± 79 s (t_{10} = 3.29, p = 0.008) for ConA and PAO, respectively. Since PAO is a blocker for pinocytosis and phagocytosis (sec. 2.4) and ConA for CME (Sec. 2.4), it is concluded that at the apex of OHCs both of these types of endocytosis could occur. Furthermore, the time delays recorded in the presence of the inhibitors are similar, indicating that the efficacy of the uptake inhibition of these blockers is not significantly different from each other.

At the base of the cell, treatment with each of the two blockers also resulted in significantly delayed FM1-43 uptake (Figure 16B). The control value of 14 ± 5 s was increased to 97 ± 51 s (t_{12} = 4.71, p = 0.0005) and 301 ± 109 s (t_{11} = 7.56, p = $1.11*10^{-5}$) for ConA and PAO, respectively. In contrast to the apex, where the time delay for both blockers was similar, at the base of OHCs the PAO-caused delay increase was found to be significantly larger than the delay increase caused by ConA (t_{11} = 4.87, p = $4.93*10^{-3}$). These data imply that at the base of OHCs the

effect of PAO was larger than that of ConA, indicating greater prevalence of phagocytosis and pinocytosis than CME at the infranuclear pole of the cell.

These data also imply that, in general, the endocytic activity at the base of the OHC is faster than at the apex of the OHC. In addition, the data also show that at the apical pole the clathrin dependent and independent processes are equally present, but at the basal pole a greater portion of membrane internalization is most probably driven by clathrin independent processes.

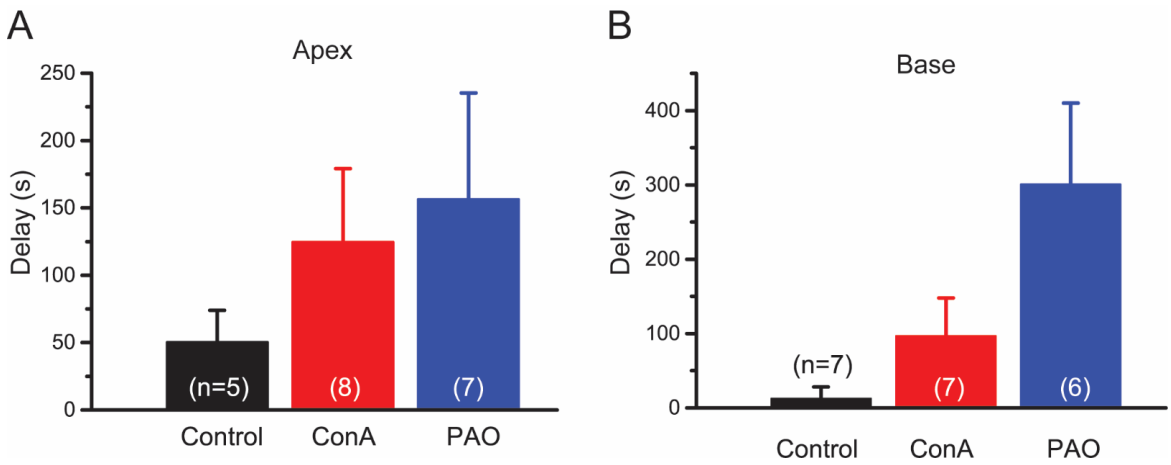

Figure 16. Uptake blockers

(A) Time after apical application for the fluorescence signals measured in the infracuticular (IC) ROI to reach the threshold for control cells (black bar), ConA treated cells (red bar) and PAO treated cells (blue bar). Number of analysed cells is indicated inside of the bars. Note that both ConA and PAO had similar and significant delay for the time needed to reach the threshold at the IC area (125 ± 55 s and. 156 ± 79 s, respectively) (B) Time after basal application for the infranuclear (IN) ROI fluorescence signals to reach the threshold for control cells (black bar), ConA treated cells (red bar) and PAO treated cells (blue bar). The time delay to the IN area for ConA and PAO were 97 ± 51 s and 301 ± 109 s, respectively. Note that PAO had significantly more effect compared to ConA (t_{11} = 4.87, p = 4.93*10^{-3}). Number of analysed cells is written either above the bar (control cells) or inside the bars (ConA and PAO).

3.5 Transcytosis blockers

In this set of experiments, the plasma membrane marker FM1-43 was applied either to the apex or to the base of the OHC to investigate the intracellular apicobasal or the basoapical dye propagation. To reveal the involvement of kinesin and myosin VI in the traffic, cells were preincubated with monastrol (Mon) and 2,4,6-Triiodophenol (TIP), respectively. The resolution of the confocal system was 1024 x 1024 pixels/frame with a scan time of at least 10 min and a scan interval of 5 sec. To measure the dye distribution along the cell, the same size ROIs were placed at an appropriate distance inside the cell, as in the case of experiments described in Sec. 3.1. The time for each ROI to reach the 20% threshold was measured and compared to control cells in the apicobasal and basoapical directions. The control cells described in Sec. 3.1 were used for comparison. Similar to Sec. 3.1, the collected data were displayed in a time-distance graph marking the time needed for each ROI to reach the threshold. The apicobasal and basoapical delays are plotted separately to emphasize the differences. To compare the dynamics of the apicobasal and the basoapical traffic, in each case the average data were fitted using linear regression with the axis-intercept set to zero.

For the apicobasal direction (Figure 17A), the Mon had no significant effect on the time to reach the threshold. However, the presence of TIP delayed the time required to reach the threshold. These observations were made for each ROI. The slope parameters were 0.119 ± 0.004 µm/s and 0.034 ± 0.001 µm/s for Mon- and TIP- treated cells, respectively. Compared to control cells, the TIP application significantly reduced the slope parameter (t_8 = 18.04, p = 9 * 10^{-8}), whereas Mon treatment had little effect (t_8 = 2.35, p = 5.14 * 10^{-2}), although just passing the $p \geq 0.05$ significance criterion. These observations indicate that from apex to base Mon had no effect on the signal increase, meaning no effect on the apicobasal FM1-43 distribution. In contrast to Mon, the presence of TIP delayed the time of each ROI to reach the threshold, indicating a reduced apicobasal intracellular dye distribution. Furthermore, data also show that the time delay relative to the plasma membrane labelling in the first ROI, that is the closest ROI placed to the expected location of endocytic activity, in the case of the TIP-treatment was significantly increased to 192 ± 40 s (t_7 = 7.5, p = 1.4*10^{-4}). That means that the dye labelled vesicles needed more time from the plasma membrane to reach the IC zone.

For the basoapical direction (Figure 17B), both blockers significantly delayed the time for each ROI to reach the threshold. The slope parameters for the Mon- and the TIP-treated cells were 0.055 ± 0.001 µm/s and 0.054 ± 0.002 µm/s, respectively. Compared to control cells, both the Mon (t_8 = 13.2, p = 1.02 * 10^{-6}) and TIP (t_8 = 13.3, p = 0.99 * 10^{-6}) significantly reduced the slope parameters. Moreover, the slope parameters for both blockers did not differ significantly from each other (t_8 = 0.78, p = 0.46). Similarly to the observations made at the apical pole, the time delay measured in the TIP-treated cells in the first (in this case the infranuclear) basal ROI relative to the plasma membrane labelling was significantly increased to 151 ± 67 s, relative to control cells (t_{11} = 5.9, p = 1.1*10^{-4}). This indicates that dye uptake at the basal pole to the infranuclear area was inhibited by TIP. Infranuclear inhibition was not observed for Mon incubated cells.

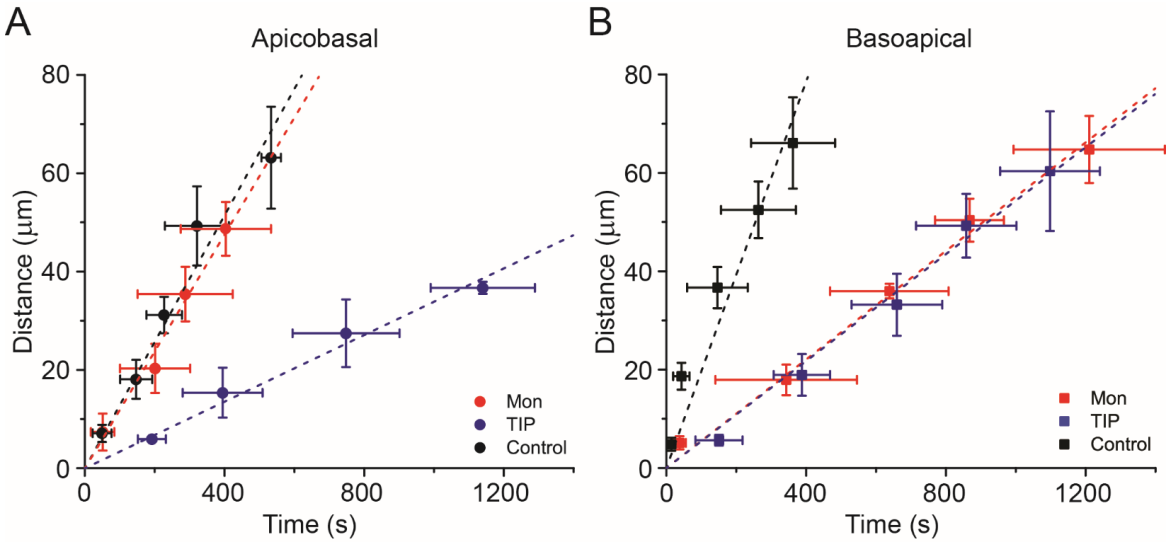

Figure 17. Transcytosis blockers

(A) Time needed for each ROI to reach the defined 20% threshold is shown for control cells (black circles), Mon treated cells (red circles) and TIP treated cells (blue circles) for traffic in the apicobasal direction. Time and distance error bars are shown in horizontal and vertical directions, respectively. Dashed lines are results of the linear regression of the average data in which the axis-intercept was set to zero. While Mon did not have a significant delay effect, TIP treatment significantly delayed the time for each ROI to reach the threshold (t_8 = 18.04, p = 9 * 10^{-8}). Note that in TIP-treated cells the first ROI exhibits also a significant time shift at the same distance.
(B) Time needed for each ROI to reach the defined 20% threshold is shown for control cells (black circles), Mon treated cells (red circles) and TIP-treated cells (blue circles) for traffic in the basoapical direction. Time and distance error bars are in horizontal and vertical directions, respectively. Both TIP and Mon caused significant delay of the traffic to each ROI. Note that Mon and TIP curves overlap and that there is also a time shift in the first ROI for TIP.

3.6 SSC-traffic vs. longitudinal traffic

In this set of experiments, the longitudinal traffic – the traffic along the longitudinal axes of the OHC – and the lateral traffic – the traffic from the central strand towards the lateral plasma membrane – were compared in control, Mon- and TIP-incubated cells. For that purpose, as in the previous experiments, circular ROIs were placed either at the M, inframiddle (IM) and SN positions or at the IC, A and M positions in the cases of apicobasal and basoapical traffic analysis, respectively (Figure 18). In

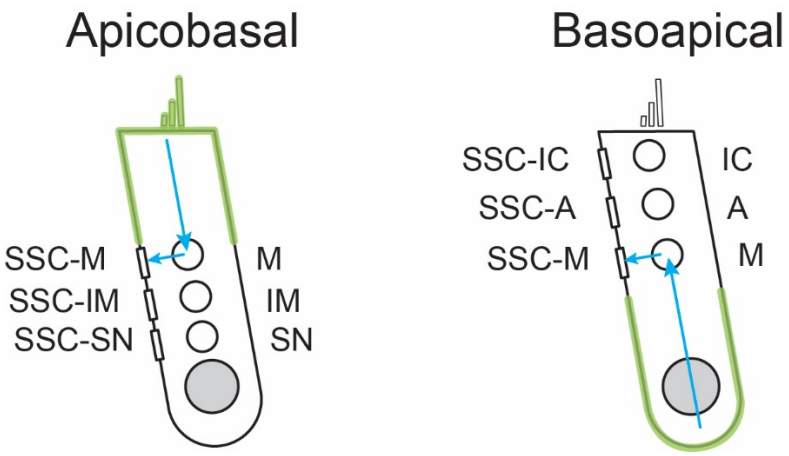

Figure 18. Location of ROIs for analyzing traffic to SSC

For the apicobasal direction, fluorescence signals were analyzed for ROIs in the cytosol locations of middle (M), inframiddle (IM) and supranuclear (SN). Time delays measured in these ROIs were compared to the time delays measured in the middle SSC (SSC-M), inframiddle SSC (SSC-IM) and supranuclear SSC (SSC-SN). For the basoapical direction, cytosolic signals of infracuticular (IC), apical (A) and middle (M) ROIs were compared to SSC signals of infracuticular SSC (SSC-IC), apical SSC (SSC-A) and middle SSC (SSC-M). Green coloured part of the cell is labelled by application of FM1-43 from one of the channels of the double-barrel capillary. Blue arrows indicate the expected route of vesicles to the middle and to the middle-located SSC of the cell.

addition to these locations, rectangular ROIs were used to evaluate signals in the SSC-plasma membrane area nearby the intracellular ROIs (Figure 18). The centrally-located circular ROI and the corresponding SSC-plasma membrane located rectangular ROI were placed always laterally opposite each other, at the same distance from the given (apical or basal) pole of the cell. ROIs to depict SSC were 1 µm thick with a length of 4 µm. The experiments were conducted in the apicobasal and basoapical directions and the double-barrel perfusion system applied to stain only one pole of the cell. Since this perfusion system stains approximately half of the outer leaflet of the lateral plasma membrane of the cell, the first ROI that could be used for analysis was always the middle of the cell. The half of the cell that was superfused with the dye could not be used because in those locations the labelling of the extracellular leaflet of the plasma membrane also contributed to the fluorescence signal recorded in the SSC ROI and could not be separated from the purely SSC labelling. In the half of the cell where the plasma membrane faced the fluid flow containing no dye molecules, the SSC ROIs contained information purely of the intracellular SSC labelling. Time delays relative to the plasma membrane labelling were calculated for the centrally-located and for the corresponding SSC-located

ROIs. Absolute and relative delays of the corresponding ROIs are shown in Figure 19. Relative delays represent the ratio of the SSC ROI time delay to the corresponding centrally-located ROI time delay. The absolute delays were determined by substracting the centrally located ROI signal delays from the corresponding SSC-located signal values. In the case of the apicobasal traffic, the ratio in control cells at M, IM and SN regions were 1.48 ± 0.22 (n = 5), 1.27 ± 0.22 (n = 5) and 1.29 ± 0.22 (n = 5), respectively. The absolute delays at these locations were 108.19 ± 63.88 s (n = 5), 67.12 ± 52.63 s (n = 5) and 78.18 ± 80.84 s (n = 5), respectively. In the case of basoapical traffic, the ratios at M, A and IC were 1.14 ± 0.49 (n = 4), 1.28 ± 0.19 (n = 5) and 1.15 ± 0.04 (n = 4), respectively. The absolute delays at these locations were 116.93 ± 95.32 s (n = 4), 80.07 ± 63.40 s (n = 4) and 46.53 ± 10.60 s (n = 4), respectively.

For Mon-treated cells and the apicobasal direction, the relative delays calculated in the M, IM and SB locations were not significantly different to the values measured in non-treated cells. However, the absolute delays for Mon-treatment at these locations were significantly different to those of the control cells (t_6 = 3.03, p = 0.02, t_6 = 5.01, p = 2.4 * 10^{-3} and t_5 = 3.19, p = 0.02). In the basoapical direction, the relative delays for the Mon-treated cells were, as in the apicobasal direction, also not significantly different to those of the control cells. In contrast to the apicobasal direction, in the basoapical direction the absolute delays were not significantly different to those of the control cells. These Mon-treatment data indicate that vesicle transport from the cell centre towards the SSC is not kinesin dependent.

For TIP-treated cells and the apicobasal direction, the middle ROI had no significant relative delay (t_7 = 1.25, p = 0.25), but in the IM and the SN locations the relative delays were significantly different to the values determined in control cells (t_7 = 4.42, p = 3 * 10^{-3} and t_7 = 3.82, p = 7 * 10^{-3}, respectively). The absolute delays for the apicobasal direction at the M, IM and SN ROIs were significantly different to control values (t_7 = 3.61, p = 9 * 10^{-3}, t_7 = 5.66, p = 8 * 10^{-4} and t_7 = 3.52, p = 0.01). In the basoapical direction, the relative delays in the A and IC ROIs were significantly different to controls (t_7 = 2.40, p = 0.05 and t_7 = 4.38, p = 3 * 10^{-3}, respectively), whereas the relative delay in the M ROI was not (t_4 = 1.24, p= 0.28). The absolute delay in that direction was significant in the A and the IC ROIs (t_7 = 3.74, p = 7 * 10^{-3} and t_7 = 4.19, p = 4 * 10^{-3}, respectively), but not in the M ROI (t_3 = 1.04, p = 0.38).

These TIP-treatment data indicate that transport to the SSC is most probably myosin VI dependent.

The absolute delay provides information about the total trafficking. Therefore, it is expected that the absolute delay increases towards the opposite end of the cell. Additionally, relative delays provide information about the lateral traffic, independent of the intracellular location along the longitudinal axis of the cell. Therefore, for the relative delays, the same values are expected along the cell being dependent only on the trafficking machinery.

Taken together, data from these SSC-traffic experiments imply that transport from the middle of the cell to the SSC is achieved through the actin-filament pathway and is therefore myosin VI dependent.

.

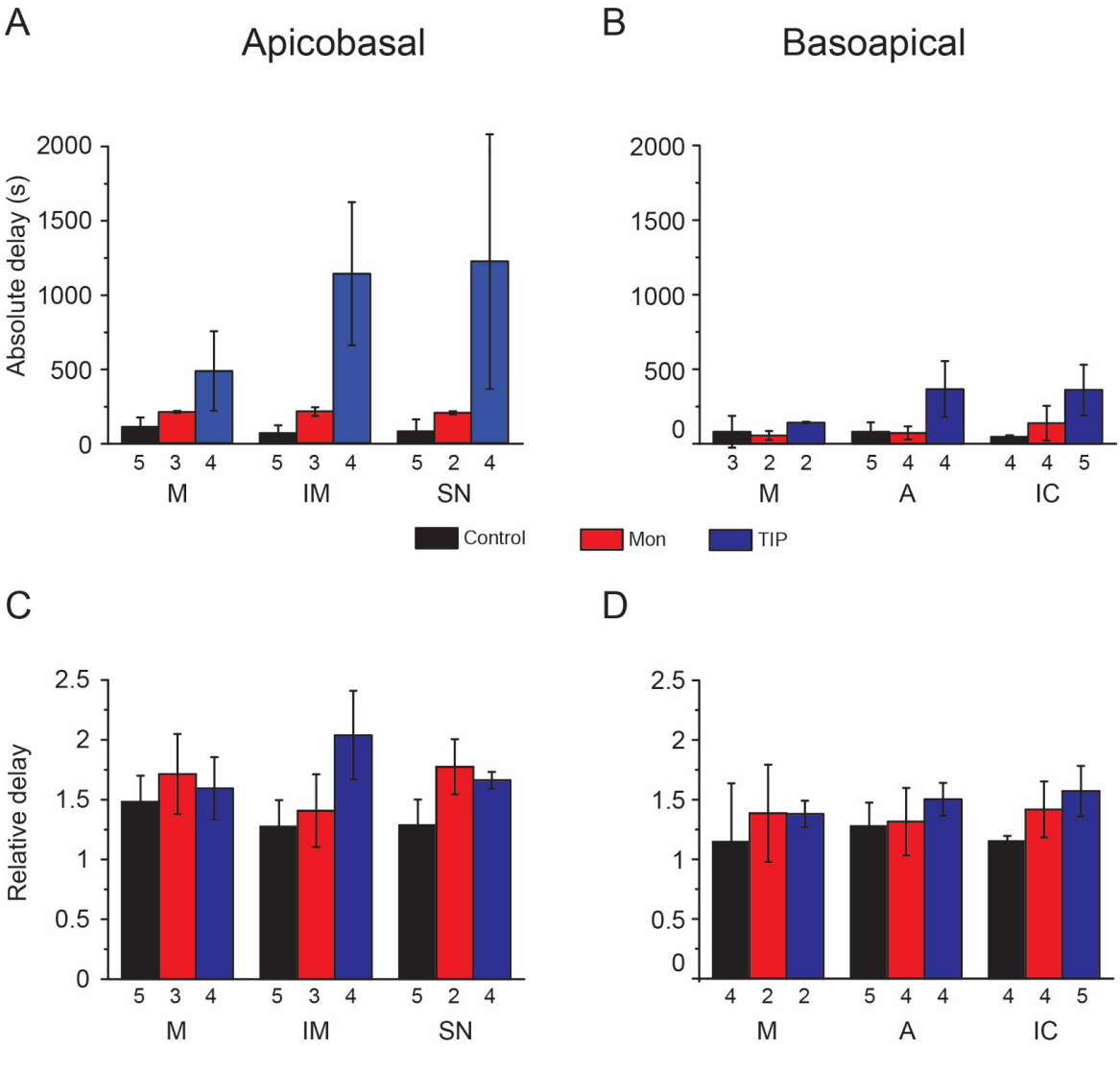

Figure 19. SSC traffic vs. longitudinal traffic

(A) Absolute and (C) relative delay for control cells (black bar), Mon-treated cells (red bar) and TIP-treated cells (blue bar) for the apicobasal direction at the locations M, IM and SN as given in Figure 18A. Both blockers significantly delayed the time to reach the threshold, although Mon-treated cells just satisfied the $p<0.05$ significance criterion. (B) Absolute and (D) relative delay for control cells (black bar), Mon-treated cells (red bar) and TIP-treated cells (blue bar) for the basoapical direction at the locations M, A and IC as given in Figure 18B. Mon-treatment had no significant effect on the absolute delay in each ROI. TIP-treated cells significantly increased the absolute delay in A and IC, but not in M. (C) Relative delays from apex to base show that Mon-treatment had no significant effect on the delay. TIP-treated cells, however, show significant relative delay in IM and SN, but not in M. (D) Relative delays from base to apex show that, as in the opposite direction, Mon treatment did not influence the relative delay. TIP-treated cells demonstrate significant relative delay in A and IC, but not in M. Numbers under the bars indicate the number of cells.

4 Discussion

Endocytic activity and vesicle traffic were investigated in OHCs isolated from the adult guinea-pig cochlea. A double-barrel perfusion system was used to stain the apical and basal parts of an isolated OHC independently (Figure 9); the system was developed in our laboratory (Harasztosi *et al.*, 2018). Using this perfusion system, it was possible to study “the apical and basal dye uptakes as well as the apicobasal and basoapical vesicle traffic independently”. (Harasztosi et al., 2018). In the first set of experiments, applying a fluorescent membrane marker solely to the apical pole of the cell, the dynamics of apical endocytosis and apicobasal traffic were compared to data of basal endocytic activity and basoapical traffic that had already been investigated in our lab (Harasztosi *et al.*, 2016). The second set of experiments was conducted to investigate the involvement of different types of endocytic activities in vesicle formation and internalization at the apex and at the base of the OHC. The third step was to determine motor proteins responsible for apicobasal and basoapical traffic. In the fourth set of experiments the MW-uptake limit of pinocytosis was investigated.

Here it is shown that both pinocytosis and clathrin-mediated endocytosis contribute to endocytic activity of OHCs. At the apex of the cell, the majority of endocytic activity was found to be clathrin-mediated, whereas at the basal pole pinocytosis and clathrin-mediated processes contributed to the total vesicle uptake, most probably equally. Data also imply that the basoapical traffic is more intense than the apicobasal traffic. Moreover, the data demonstrate that the apicobasal traffic route is kinesin independent and mainly based on the motor protein myosin VI, while the basoapical route contains both the myosin VI and the kinesin driven mechanisms. The results are summarized schematically in Figure 20.

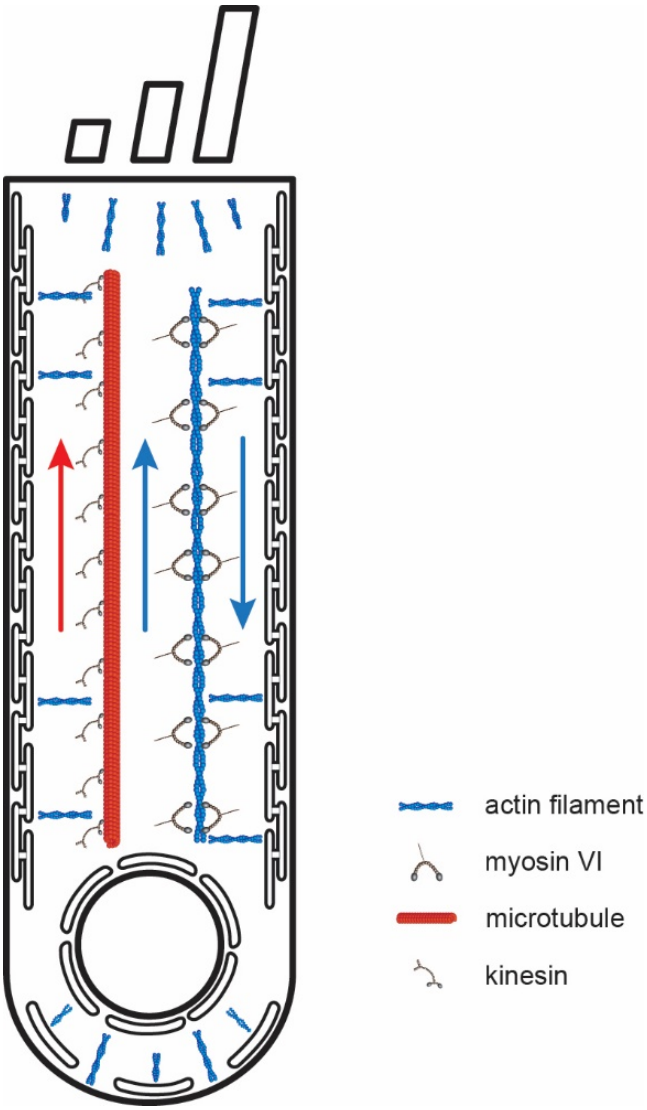

Figure 20. Summary of uptake and transport mechanisms

Schematic diagram demonstrating the transcytosis mechanisms in the OHC. Blue double helical structure represents the actin filaments. Blue arrows show the direction of movement of the microfilament motor protein myosin VI. Red tubular structure represents the microtubules. Red arrow shows the traffic direction of the microtubule motor protein kinesin. Traffic to the SSC (black structure near the lateral wall) is mediated by myosin VI, represented by blue horizontal lines.

4.1 Types of endocytosis in hair cells

Different types of endocytosis are responsible for molecule internalization in eukaryotic cells (Alberts *et al.*, 2015). Clathrin-coated vesicles as well as non-clathrin-coated vesicles have been demonstrated at the apical pole of bullfrog vestibular hair cells (Kachar *et al.*, 1997). The presence of clathrin-coated vesicles could be also shown at the basal pole of OHCs using electron microscopy (Nadol, 1983). Due to the high rate of endocytosis the consensus up to now was that mostly non-clathrin-mediated endocytosis is responsible for molecule internalization of hair cells (Griesinger *et al.*, 2002; 2004). However, recently it was shown that endocytosis could be inhibited by the dynamin blocker, Dynasore, in IHCs (Duncker *et al.*, 2013), implying a significant presence of a clathrin-mediated uptake mechanism in IHCs. However, this hypothesis is tentative because of the quenching effect of Dynasore on the fluorescence marker, making artefact-free fluorescence detection impossible (Alharazneh *et al.*, 2011; Harasztosi *et al.*, 2018).

Therefore, here, the presence of different types of endocytic activities was investigated at the opposite poles of OHCs using the pinocytosis/phagocytosis blocker PAO (Gibson *et al.*, 1989) and the clathrin-mediated endocytosis inhibitor ConA (Luttrell *et al.*, 1997). It was found that both PAO and ConA resulted in significant signal delay at both poles of the OHC in comparison to control cells (Figure 16). These data imply that both clathrin-mediated and the non-clathrin-mediated endocytic mechanisms are present at both poles of the OHC. Furthermore, the data suggested a mostly clathrin-mediated process at the apical pole of the OHC. At the base of the cell, although both blockers caused signal delay, the PAO evoked signal delay was significantly longer that the time delay caused by the ConA. Therefore, it is concluded that at the base of the OHC both clathrin-mediated and non-clathrin-mediated processes are present contrasting to the apical pole of the cell.

4.2 Pinocytosis MW-uptake limit

It is known that there are different uptake mechanisms for molecule internalization in eukaryotic cells (Alberts *et al.*, 2008). In epithelial cells, clathrin-mediated as well as non-clathrin-mediated endocytosis, such as pinocytosis, have been described as the uptake mechanisms at the apex and at the base (Apodaca, 2001b). It is not clear whether OHCs also internalize macromolecules by pinocytosis like other epithelial cell types such as the intestinal epithelia, where the uptake of the fluid-phase markers Lucifer Yellow and fluorescent dextran has been demonstrated (Hidalgo *et al.*, 1989). In the present study, fluid-phase markers in the molecular-weight range of 500 to 10,000 Da were used in order to quantify the upper size/weight limit of molecules that can be internalized via pinocytosis. The results show that neither Dextran Oregon Green® 514 (MW= 10,000 Da) nor Lucifer Yellow (MW= 521 Da) were taken up by OHCs, even when the measurement time was extended to 30 minutes (Figure 13), which is sufficient for pinocytosis to occur (Ryan *et al.*, 1996). Therefore, it is assumed that the molecular weight of pinocytosed molecules can be no larger than 500 Da to be able to be endocytosed by OHCs. This conclusion disagrees with a previous study, where the uptake of Lucifer Yellow was investigated and staining was found to be similar to that of FM1-43 (Griesinger *et al.*, 2004). However, in that study, Lucifer Yellow was applied in a much higher concentration (20 mM) than FM1-43 (5 µM). In the present study, the concentrations of FM1-43 and Lucifer Yellow were 10 µM and 50 µM, respectively, similar to that of FM1-43. Therefore, this discrepancy between the two different studies could result from the extreme difference between the concentrations of the applied markers. Lucifer Yellow is negatively charged and Dextran Oregon Green® 514 positively charged. Therefore, the possibility of uptake being influenced by the net charge of the fluid-phase markers was tested by manipulating the transmembrane potential using the patch-clamp technique. It was found that depolarization did not affect the uptake of Lucifer Yellow. The experiment was not performed for Dextran Oregon Green® 514 because that fluorescent marker is positively charged. Although no fluid-phase marker has been found that could be endocytosed by isolated OHCs, our data imply that the MW limit for pinocytosis must be less than 500 Da for OHCs.

One explanation for the difference in OHCs compared to other epithelial cells, where larger molecules can be internalized (Menard *et al.*, 2010), might be the

different physiological roles of endocytosis. In intestinal epithelial cells, endocytosis is mainly used to internalize nutrients, which in OHCs would not be the primary role since there is no direct nutrition pathway known through which they could be delivered to the cell. However, it is possible that lipid droplets could enter OHCs via pinocytosis. It has been shown that Hensen's cells, which are neighbouring cells to the OHCs, produce lipid droplets possessing well-known molecular components to be able to accelerate and enhance the resolution phase of inflammatory responses (Urrutia & Kalinec, 2015). Lipid droplets belong to those substances which are taken up via pinocytosis and inside the cell exhibit energy delivering properties (Thiam *et al.*, 2013). Lipid droplets exist in various sizes: from small in size lipid droplets in yeast to larger in white adipocytes; the factors involved in size determination are not fully agreed upon (Tan *et al.*, 2014). Since lipid droplets function as energy carriers, it might be possible that they contribute to such functions of the OHC.

Another possibility would be to test whether ototoxic antibiotics, e.g. aminoglycosides could enter the OHC via pinocytosis and cause irreversible damage. Although it has been postulated that these antibiotics enter the hair cells via the MET-channels (Alharazneh *et al.*, 2011), there is not yet a clear consensus whether that is the case. It is known that aminoglycosides have varying molecular weight between 446 and 600 Da. Therefore, aminoglycosides with less than 500 Da molecular weight, like gentamicin (477 Da), might be taken up by the OHC via pinocytosis. In the present study, a maximal uptake limit for pinocytosis was established (<500 Da), which is informative for therapeutics targeting locations inside the OHC. If it is known that pharmaka which enter the cell via pinocytosis are smaller than 500 Da, one might suspect that they could enter the cell and fulfil their therapeutic destination.

Another possibility would be that adaptor proteins are the incoming molecules to the OHC. It has been reported that these proteins with the clathrin complex are excluded from the stereocilia and restricted to the pericuticular apical membrane (Grati *et al.*, 2006). It was proposed that due to the enrichment of adaptor proteins in the apical membrane of the OHC, the plasma-membrane adaptor proteins and therefore clathrin-mediated processes might be responsible for the exchange and removal of membrane proteins between the stereocilia at the periphery of the apical cell surface, resulting in a constant rapid membranous turnover (Grati *et al.*, 2006). Further experiments are necessary to determine the MW upper limit for endocytosed

vesicles and the exact molecular identity of the molecules which are being pinocytosed *in vivo*.

4.3 Intracellular targets of basally endocytosed vesicles

From previous studies it is known that apically endocytosed vesicles in the OHC traffic to different intracellular compartments, e.g. the apical endosome, the apical compartment, the central compartment as well as the basal compartment (Griesinger *et al.*, 2004) and even to the infranuclear pole and the basolateral wall (Meyer *et al.*, 2001; Kaneko *et al.*, 2006). In these studies (Griesinger *et al.*, 2004; Kaneko *et al.*, 2006), the fluorescent membrane marker FM1-43 was applied to the apex of the cell and intracellular targets, using colocalization with $DiOC_6$, of apically endocytosed vesicles were investigated. However, for basal application of FM1-43, intracellular destinations were still an enigma. Therefore, in the present study, the base to apex distribution of the fluorescent probe was investigated after preincubating the OHC in $DiOC_6$. This fluorescent marker is used to label the ER and mitochondria (Terasaki, 1989; Terasaki & Reese, 1992; Koning *et al.*, 1993). $DiOC_6$ exhibits strong phototoxicity (Pettit & Hallett, 1998), which leads to bleaching of the $DiOC_6$ if it is exposed for too long to the laser beam. To minimize phototoxicity, $DiOC_6$ was used in low concentrations (0.87 µM) similar to a previous study (Kaneko *et al.*, 2006), and the incubation time was limited to 1 min. After incubation in $DiOC_6$, the membrane marker FM4-64 was applied to the basal half of the cell and colocalization with $DiOC_6$ was examined (Figure 15). Basally endocytosed vesicles were found to colocalize with the ER and mitochondria, suggesting that these intracellular organelles might be a common destination of not only apically but also basally endocytosed cargo.

Another characteristic of the colocalization experiments was that, in time, the FM4-64 staining became more apparent, whereas the $DiOC_6$ staining vanished. This effect could have been partially due to the phototoxic properties of the ER-marker. However, that could not be proven because shorter scanning intervals, which would result in less phototoxicity, did not reduce the apparent vanishing effect. A more obvious explanation of the observed vanishing of the $DiOC_6$-labelling is that an

interaction between the different types of dye molecules could have occurred. There is a known mechanism called Förster resonance energy transfer (FRET), which would explain these events. FRET is the process of energy transfer from a donor to an acceptor fluorophore, which exhibit overlapping excitation/emission fluorescent spectra (Förster, 1982; Moussa, 2012). The fluorescent membrane markers FM1-43 and FM4-64 have been described to display such FRET-interaction, in which FM4-64 quenches the fluorescence of FM1-43 (Cochilla *et al.*, 1999; Duncan *et al.*, 2004). The reason for this interaction is that the emission spectrum of the donor overlaps with the excitation spectra of the acceptor fluorophore, thereby causing energy shift from the donor to the acceptor. This FRET-interaction could also be active in the present experiments. Since $DiOC_6$ has an excitation spectrum of 400 - 520 nm and an emission spectrum of 475 - 650 nm and FM1-43 has an excitation spectrum of 365 - 580 nm and an emission spectrum of 500 - 720 nm, their excitation/emission spectra overlap. Therefore, it stands to reason that $DiOC_6$ might have acted as the donor fluorophore and FM4-64 as the acceptor fluorophore. However, FRET does not influence the colocalization results because the dyes can only interact if they are in the same location. Nevertheless, precautions were made to reduce the bleaching effect, so that from the results of the experiments it can be concluded that basally endocytosed vesicles labelled with FM4-64 were colocalized with $DiOC_6$, and, therefore, with the ER and the mitochondria in OHCs.

4.4 Apicobasal vs. basoapical traffic

In eukaryotic cells it is known that the cytoskeleton is involved in the transport of cargo along the cell (Kelly, 1990). In epithelial cells which are polarized – they have an apical pole and a basal pole –, the cytoskeleton also plays a major role in the transport along the cell in order to maintain their polarity (Mays *et al.*, 1994). In the current study, apicobasal traffic is defined as the traffic from the apex towards the base and basoapical as from the base towards the apex, including but not limited to the cytoskeleton and its motor proteins. Until now, little was known about the dynamics of apicobasal and basoapical traffic in the OHC.

In a previous study, the apicobasal and the basoapical traffic were compared by applying different fluorescent membrane markers to both poles of the cell (Harasztosi *et al.*, 2016). The double-barrel perfusion system was used to double label isolated OHCs. FM1-43 was applied at the apical pole, whereas FM4-64 was applied at the basal pole. In that study, additional data for the basoapical traffic was gathered from solely basally labelled cells, whereas data for the apicobasal traffic was acquired from double-labelled cells. It was found that the basoapical traffic is faster than the apicobasal traffic. However, there were no control cells with solely apical uptake of fluorescent markers. Therefore, in the first experiments of the present study, OHCs were labelled with fluorescent membrane markers at their apical pole to investigate and compare the dynamics of apicobasal traffic to that of basoapical traffic. Therefore, in this study, isolated OHCs were labelled exclusively at the apex using double-barrel perfusion and the collected data compared to that of basoapical traffic in basally stained cells. Data show significant difference in apicobasal and basoapical speed, namely that the traffic towards the apex is faster, being 0.129 ± 0.007 μm/s as opposed to 0.196 ± 0.015 towards the base (Figure 12). This is a confirmation of the previously suggested speed difference of apicobasal and basoapical traffic (Harasztosi *et al.*, 2016). These speeds compare with those in other systems: 1) *in vitro* velocity of dynein in porcine brain cells is 0.8 μm/s (Toba *et al.*, 2006) and 2) in axon, speeds of different transport proteins (plasma membrane proteins, synaptic vesicle proteins, and trans-Golgi network residual proteins) range from 0.69 to 0.98 μm/s (Nakata *et al.*, 1998).

The data are also consistent with previous studies, where the uptake rates at the apex and base have been identified as different (Harasztosi *et al.*, 2014). The speed of apicobasal traffic in OHCs has been reported to be 0.36 ± 0.03 μm/s (Kaneko *et al.*, 2006), which is similar to results from another study of our group (Harasztosi *et al.*, 2016). In the present study, the first ROI in the apicobasal direction showed a time delay to the plasma membrane of 50 ± 23 s, whereas the time delay in the first ROI in the basoapical direction was 14 ± 5 s. These values are significantly different. Since the distances from the plasma membrane to the infranuclear and the infracuticular ROIs in all cells were ~6 μm and ~7 μm, respectively, the difference in time delay in the first ROI after internalization is most probably due to differences in uptake rate at these poles. At the base of the OHC the

uptake speed was 0.196 ± 0.015 µm/s in the basoapical direction and 0.129 ± 0.007 µm/s at the apex in the apicobasal direction (Figure 12).

An explanation as to why the traffic speed in the opposite directions and uptake at the opposite poles are different could be the different morphological structures present at the apex and base. At the apex of OHCs, there is a high concentration of microtubules, whereas at the base of OHCs their concentration is lower (Sec. 1.2.2). It is, therefore, likely that in the basoapical direction other transport mechanisms exist, which are faster than transport along the apicobasal route. Another explanation could be that different types of uptake, which differ in speed, are present at the apex and base of the cell. The types involved in apical and basal uptake, as well as the transport mechanisms in the apicobasal and basoapical directions, are discussed in the following sections.

4.5 Types of transcytosis

The next set of experiments focused on determining the transportation pathways of cargo, which is endocytosed in the apicobasal and basoapical directions. Generally, there are mainly two different pathways of vesicle traffic inside eukaryotic cells: the microtubules and the actin filaments (Sec. 1.4.1). Epithelial cells are special in that the minus end of microtubules is located towards the apex and the minus end of microfilaments is located away from the plasma membrane towards the nucleus. The motor proteins responsible for traffic along these pathways, apart from dynein, are kinesin and myosin VI. Kinesin is one of the motor proteins of the microtubules and myosin VI that of the actin filaments (Sec. 1.4.1). In a previous study monastrol, a kinesin inhibitor, was used in IHCs and showed significantly reduced fluorescence intensity from apex to base (Griesinger *et al.*, 2002). The myosin VI inhibitor TIP is known to be an efficient blocker of myosin VI (Heissler *et al.*, 2012). Therefore, the effects of TIP and monastrol, blockers of these motor proteins, on the intracellular transport of vesicles were investigated.

The kinesin inhibitor monastrol did not significantly delay transport in the apicobasal direction compared to control cells (Figure 17A). However, monastrol caused significant signal delay in the basoapical direction (Figure 17B). Therefore, it

is concluded that transport is kinesin-dependent only in the basoapical direction (Figure 20).

The myosin VI inhibitor TIP increased signal delay in both the apicobasal and the basoapical directions (Figure 17). Therefore, it is concluded that both the apicobasal and the basoapical trafficking are myosin VI dependent processes (Figure 20). Another explanation of the observations could be that myosin IV is responsible only for vesicle traffic from the surface membrane to the first endosome while kinesin is responsible for the traffic along the OHC towards the apex.

These results are consistent with the minus end of microtubules in epithelial cells, such as OHCs, being located at the apex of the cell (Sec. 1.6.1), therefore suggesting that kinesin is responsible for moving cargo only in the basoapical direction. This result has already been reported and shown in Madin-Darby canine kidney cells (Bacallao *et al.*, 1989). However, it has also been shown that kinesin is responsible not only for basoapical traffic, but also for moving cargo bidirectionally depending on the position of the motor domain of this protein (Endow & Higuchi, 2000). Specifically, kinesins with N-terminal motor domains move their cargo towards the plus ends of microtubules, while kinesins with C-terminal motor domains move cargo towards the minus ends of microtubules (Endow & Barker, 2003; Marx *et al.*, 2009). Interestingly, the results of the present study suggest that in the OHC kinesin is responsible mainly for the basoapical vesicle distribution, meaning that kinesins with C-terminal motor domains contribute largely to the basoapical traffic in this type of cell. It has also been shown that a population of microtubule minus ends is anchored at the most-apical part of the cadherin-based adherent junction of epithelial cells (Meng *et al.*, 2008). The present data suggest that the minus end of actin transporter myosin VI is responsible for moving cargo in both the apicobasal and basoapical directions, implying that actin filaments are oriented in both directions along the longitudinal axes of the OHC. However, as mentioned in the last paragraph, it cannot be ruled out that myosin IV is responsible for vesicle transport from the plasma membrane to the first endosome. Therefore, the observed reduced trafficking speed in the presence of the myosin IV blocker might be related to the reduced uptake.

It has already been shown that myosin VI is responsible for this beginning of the traffic pathway in epithelial cells in general (Tumbarello *et al.*, 2013). In IHCs it has been shown that myosin VI is responsible for traffic in the stereocilia (Hertzano

et al., 2008). However, until now no such investigations had been conducted in OHCs. The increased signal delay at the first ROI for OHCs incubated in TIP but not Mon (Figure 17) suggests that myosin VI is responsible for the traffic towards the first basal and apical intracellular destination of vesicles in OHCs.

In the future, it will be of great interest to investigate the role of other motor proteins, such as dynein, in the intracellular traffic dynamics in the OHC.

4.6 SSC-traffic

Although most of the transport in epithelial cells is active transport to different intracellular destinations, there is the possibility of lateral traffic in the cell. Lateral traffic is the transport of vesicles from the centre of the cell to the lateral membrane. In this study, in order to investigate this lateral SSC traffic, the time needed to reach a certain individual threshold in the SSC was compared to the longitudinal traffic in control cells and afterwards also to the transport in cells treated with traffic blockers. In control cells, for the basoapical direction as well as in apicobasal direction, there was a delay for the SSC to reach the defined threshold (Figure 19). Furthermore, the ratio of longitudinal traffic time and SSC-traffic time was found out to be consistently ~1.4. This indicates that the fluorescently labelled vesicles first traffic along the central strand towards different intracellular destinations and from there are transported to the SSC (Figure 20). In OHCs, it is known that actin filaments are distributed as in other epithelial cell types (Raphael *et al.*, 1994), namely that they extend from the central strand towards the lateral plasma membrane. In epithelial cells, myosin VI has been reported to be responsible for adaptor protein (AP)-1B-dependent cargo to the basolateral domain (Au *et al.*, 2007). Therefore, the influence of the myosin VI blocker TIP on the lateral traffic was tested in both directions. Using the kinesin inhibitor monastrol, it was further investigated whether the lateral transport could be also kinesin dependent.

For either apical or basal application of FM1-43, monastrol did not significantly affect the relative delay, that is, the delay to the SSC ROI relative to the delay to the directly opposed central ROI (Figure 19C, D). The relative delays in both directions

were not significantly different. In contrast, there was a small but significant increase in the absolute delay between the SSC ROI and the central ROI for the apical application of FM1-43 (Figure 19A, B). However, considering the results for the transcytosis experiments (Figure 17), where Mon-treated cells did not affect the apicobasal traffic (Sec. 3.5) and based on the relative delays to the SSC, it is concluded that Mon did not significantly affect transport to the SSC. In other words, the lateral traffic to the SSC does not appear to be kinesin-dependent (Figure 20).

For either apical or basal application of FM1-43, the myosin VI inhibitor TIP significantly affected the traffic in all of the placed ROIs except the middle (Figure 19C, D). TIP significantly affected the traffic in each ROI (Figure 19A, B). Therefore, it is concluded that in the infracuticular, the apical, the inframiddle and the supranuclear areas of the OHC, TIP reduced the transport to the SSC, meaning that this lateral traffic is myosin VI dependent (Figure 20). It is further concluded that in the middle of the cell there might be little-to-no myosin VI-mediated transport to the SSC.

4.7 Conclusion

At the apical pole of the OHC, endocytosis appears to be mainly clathrin-mediated, whereas at the basal pole, where the uptake is more intense, pinocytosis and clathrin-mediated processes contribute equally to the uptake. The uptake of molecules by the OHC via pinocytosis is restricted to molecules no larger than a molecular weight of 500 Da. Vesicles endocytosed at the basal pole traffic towards the endoplasmic reticulum and the mitochondria and vesicles endocytosed at the apical pole to the SSC and basal pole.

The vesicle traffic towards the apex is faster than towards the base. Both apicobasal and basoapical transcytosis are myosin VI dependent and the traffic in the basoapical direction is also kinesin dependent. Myosin VI is responsible for vesicle traffic between the plasma membrane, the site of vesicle formation, and the first apical as well as the first basal vesicle destination after endocytosis. All along the cell, myosin VI was found to be responsible for the lateral traffic from the central strand to the SSC, except in the middle of the cell.

5 Summary

In the present study, endocytosis and transcytosis mechanisms were investigated in the bipolar OHC. This type of epithelial cell, located in the organ of Corti, contributes to the amplification of sound. As a key feature of epithelial cells, endocytosis is responsible for altering the biochemical composition inside the cell. Upon entering the cell, cargo is transported via motor proteins along different pathways to its required intracellular destination, through the process called transcytosis. Until now, in the OHC most of the research was focused on investigating the apical pole and destinations of apically endocytosed product. The prevalent uptake mechanism at each pole as well as the traffic pathways and motor proteins involved in cargo movement, had not been investigated.

Therefore, the goal of this study was to clarify the endocytosis and transcytosis processes in the OHC. For endocytosis experiments, the aim was to elucidate the different types of endocytosis present at both poles, using blockers of different types of internalization, as well as to quantify the molecular-weight limit of molecules which can be internalized. Since intracellular targets of basally endocytosed product were not yet clear, in another set of experiments the destinations of basally endocytosed vesicles were investigated. For transcytosis experiments, the aim was to compare the dynamics and pathways of apicobasal and basoapical vesicle traffic. Using blockers, another goal was to investigate the participation of motor proteins in vesicle traffic. In the last set of experiments, processes to the SSC were compared to those along the cell.

To apply fluorescent markers to exclusively one pole of the cell, a newly developed double-barrel perfusion system was used. Visualizing the uptake and intracellular dye distribution was enabled through confocal laser scanning microscopy. Additional patch clamp experiments were performed to investigate whether uptake might be charge dependent.

Basal uptake was more intense than apical uptake. Furthermore, at the apex the principle uptake mechanism was clathrin-mediated endocytosis, whereas at the base internalization was both non-clathrin mediated and the clathrin-mediated. Pinocytosis was restricted to molecules no larger than 500 Da. It was found that upon entering the OHC through the basal pole of the cell, vesicles traffic towards the

ER and the mitochondria. The basoapical traffic was faster than the apicobasal traffic. Both basoapical and apicobasal traffic was myosin VI dependent, whereas only the traffic from apex to base was kinesin dependent. The first destinations after internalization at the apex and base of the OHC were myosin VI dependent. Endocytosed vesicles trafficked first along a longitudinal axis to the central areas of the cell and then were transported to the SSC. The SSC traffic appeared to be mainly myosin VI dependent.

In summary, in this study it is demonstrated for the first time which uptake mechanisms dominate at the apical and the basal pole and which motor proteins are involved in traffic along the cell and to the SSC. The molecular identity of endocytosed and transcytosed material *in vivo* has yet to be identified.

6 Zusammenfassung

In der vorliegenden Studie wurden Endozytose- und Transzytose-Mechanismen der bipolaren äußeren Haarzelle (ÄHZ) untersucht. Diese Art von Epithelzelle, welche sich im Corti'schen Organ befindet, trägt zu der Amplifikation des Tones bei. Endozytose ist als wesentlicher Mechanismus in Epithelzellen dafür verantwortlich, zellfremdes Material in die Zelle aufzunehmen. Nach Eingang in die Zelle wird Cargo durch Transzytose mit Hilfe von Motorproteinen entlang verschiedener Wege transportiert, um zu bestimmten intrazellulären Destinationen zu gelangen. Bislang war der Großteil an Forschungen an der ÄHZ auf den apikalen Pol und dessen endozytierte intrazelluläre Destinationen fokussiert. Die vorherrschenden Aufnahmeprozesse an den jeweiligen Polen sowie die Transportwege und involvierten Motorproteine wurden bislang jedoch bislang nicht untersucht.

Das Ziel dieser Studie war daher, die Endozytose- und Transzytose-Prozesse in der ÄHZ näher zu erläutern. Das Ziel in den Endozytoseexperimenten war, mit Hilfe von unterschiedlichen Aufnahmeblockern, die verschiedenen Typen von Endozytose an jedem Pol zu erläutern und darüber hinaus die Molekulargewichtsgrenze für mögliche internalisierte Moleküle zu quantifizieren. Da die intrazellulären Ziele von basal aufgenommenen Molekülen nicht bekannt sind, wurden in einer weiteren Experimentreihe diese untersucht. Das Ziel in den Transzytoseexperimenten war, die Dynamik sowie die Transportwege von apikobasalen und basoapikalen Vesikeln zu vergleichen. Durch den Einsatz von verschiedenen Blockern von Motorproteinen, wurde deren Mitbeteiligung am Vesikeltransport untersucht. In der letzten Experimentreihe wurden Transportwege zu den subplasmaren Zisternen mit denen entlang der Zelle verglichen.

Um Fluoreszensmarker ausschließlich an einem Pol der Zelle zu applizieren, wurde eine neu entwickeltes Zwei-Kammer Perfusionssystem angewendet (Harasztosi *et al.* 2018). Die Visualisierung der Aufnahme und Distribution der Farbstoffe wurde mittels konfokaler Lasermikroksopie realisiert. Zusätzliche wurden Patch-Clamp-Experimente durchgeführt, um zu untersuchen, ob die Molekülaufnahme ladungsabhängig seien könnte.

Die basale Aufnahme von Molekülen war intensiver als die apikale. Darüber hinaus herrschten überwiegend clathrin-übermittelte Aufnahmemechanismen am Apex der Zelle, wohingegen an der Basis ebenfalls clathrin-unabhängige Endozytose vorlag. Pinozytose war auf Moleküle mit Molekulargewicht weniger als 500 Da beschränkt. Nach Aufnahme in die Zelle über den basalen Pol, bewegten sich Vesikel zum endoplasmatischen Retikulum und den Mitochondrien. Der basoapikale Transport war schneller als der apikobasale. Sowohl basoapikaler als auch apikobasaler Transport waren myosin-VI-abhängig, wohingegen nur der Transport von Apex nach Basis kinesin-abhängig war. Die ersten Destinationen nach Internalisierung am Apex und der Basis der Zelle waren myosin-VI-abhängig. Endozytierte Vesikel bewegen sich nach Aufnahme zuerst entlang einer longitudinalen Axis zu den zentralen Arealen der Zelle und von dort in Richtung der subplasmaren Zisternen. Dieser laterale Transport war höchstwahrscheinlich myosin-VI-abhängig.

Zusammenfassend wurde in dieser Studie zum ersten Mal gezeigt welche Aufnahmemechanismen jeweils am apikalen und basalen Pol dominieren und welche Motorproteine in dem Transport entlang der Zelle und in Richtung der subplasmaren Zisternen involviert sind. Die molekulare Identität der endozytierten und transzytierten Produkte *in vivo* sind noch zu erforschen.

7 References

Alberts, B., Johnson, A., Lewis, J., Morgan, D., Raff, M., Roberts, K., Walter, P., Wilson, J. & Hunt, T. (2015) *Molecular Biology of the Cell*. New York, Garland Science.

Alberts, B., Johnson, A., Lewis, J., Raff, M., Roberts, K. & Walter, P. (2008) Intracellular vesicular traffic. *Molecular Biology of the Cell*. New York, Garland Science, pp. 711–766.

Alharazneh, A., Luk, L., Huth, M., Monfared, A., Steyger, P.S., Cheng, A.G. & Ricci, A.J. (2011) Functional hair cell mechanotransducer channels are required for aminoglycoside ototoxicity. *PLoS One*, **6**, e22347.

Apodaca, G. (2001a) Endocytic traffic in polarized epithelial cells: role of the actin and microtubule cytoskeleton. *Traffic*, **2**, 149–159.

Apodaca, G. (2001b) Endocytic traffic in polarized epithelial cells: role of the actin and microtubule cytoskeleton. *Traffic.*, **2**, 149–159.

Apodaca, G., Gallo, L.I. & Bryant, D.M. (2012) Role of membrane traffic in the generation of epithelial cell asymmetry. *Nat Cell Biol*, **14**, 1235–1243.

Arnold, W. & Anniko, M. (1990) Structurally based new functional interpretations of the subsurface cisternal network in human outer hair cells. *Acta Otolaryngol*, **109**, 213–220.

Au, J.S., Puri, C., Ihrke, G., Kendrick-Jones, J. & Buss, F. (2007) Myosin VI is required for sorting of AP-1B-dependent cargo to the basolateral domain in polarized MDCK cells. *J Cell Biol*, **177**, 103–114.

Bacallao, R., Antony, C., Dotti, C., Karsenti, E., Stelzer, E.H. & Simons, K. (1989) The subcellular organization of Madin-Darby canine kidney cells during the formation of a polarized epithelium. *J Cell Biol*, **109**, 2817–2832.

von Békésy, G. (1960) Experiments in Hearing. *New York: McGraw-Hill*.

Betz, W.J. & Bewick, G.S. (1992) Optical analysis of synaptic vesicle recycling at the frog neuromuscular junction. *Science*, **255**, 200–203.

Beurg, M., Fettiplace, R., Nam, J.H. & Ricci, A.J. (2009) Localization of inner hair cell mechanotransducer channels using high-speed calcium imaging. *Nat Neurosci*, **12**, 553–558.

Beutner, D., Voets, T., Neher, E. & Moser, T. (2001) Calcium dependence of exocytosis and endocytosis at the cochlear inner hair cell afferent synapse. *Neuron*, **29**, 681–690.

Bhabha, G., Johnson, G.T., Schroeder, C.M. & Vale, R.D. (2016) How Dynein Moves Along Microtubules. *Trends Biochem Sci*, **41**, 94–105.

Bolte, S., Talbot, C., Boutte, Y., Catrice, O., Read, N.D. & Satiat-Jeunemaitre, B. (2004) FM-dyes as experimental probes for dissecting vesicle trafficking in living plant cells. *J Microsc*, **214**, 159–173.

Bond, L.M., Tumbarello, D.A., Kendrick-Jones, J. & Buss, F. (2013) Small-molecule inhibitors of myosin proteins. *Future Med Chem*, **5**, 41–52.

Brownell, W.E., Bader, C.R., Bertrand, D. & de Ribaupierre, Y. (1985) Evoked mechanical responses of isolated cochlear outer hair cells. *Science*, **227**, 194–196.

Buss, F., Luzio, J.P. & Kendrick-Jones, J. (2002) Myosin VI, an actin motor for membrane traffic and cell migration. *Traffic*, **3**, 851–858.

Buss, F., Spudich, G. & Kendrick-Jones, J. (2004) Myosin VI: cellular functions and motor properties. *Annu Rev Cell Dev Biol*, **20**, 649–676.

Cochilla, A.J., Angleson, J.K. & Betz, W.J. (1999) Monitoring secretory membrane with FM1-43 fluorescence. *Annu Rev Neurosci*, **22**, 1–10.

Cramer, L.P. (1999) Organization and polarity of actin filament networks in cells: implications for the mechanism of myosin-based cell motility. *Biochem Soc Symp*, **65**, 173–205.

Duncan, R.R., Bergmann, A., Cousin, M.A., Apps, D.K. & Shipston, M.J. (2004) Multi-dimensional time-correlated single photon counting (TCSPC) fluorescence lifetime imaging microscopy (FLIM) to detect FRET in cells. *J Microsc*, **215**, 1–12.

Duncker, S.V., Franz, C., Kuhn, S., Schulte, U., Campanelli, D., Brandt, N., Hirt, B., Fakler, B., Blin, N., Ruth, P., Engel, J., Marcotti, W., Zimmermann, U. & Knipper, M. (2013) Otoferlin couples to clathrin-mediated endocytosis in mature cochlear inner hair cells. *J Neurosci*, **33**, 9508–9519.

Dutta, D. & Donaldson, J.G. (2012) Search for inhibitors of endocytosis: Intended specificity and unintended consequences. *Cell Logist*, **2**, 203–208.

Endow, S.A. & Barker, D.S. (2003) Processive and nonprocessive models of kinesin movement. *Annu Rev Physiol*, **65**, 161–175.

Endow, S.A. & Higuchi, H. (2000) A mutant of the motor protein kinesin that moves in both directions on microtubules. *Nature*, **406**, 913–916.

Fischer-Parton, S., Parton, R.M., Hickey, P.C., Dijksterhuis, J., Atkinson, H.A. & Read, N.D. (2000) Confocal microscopy of FM4-64 as a tool for analysing endocytosis and vesicle trafficking in living fungal hyphae. *J Microsc*, **198**, 246–259.

Förster, T. (1982) *Fluoreszenz organischer Verbindungen*. Vandenhoeck & Ruprecht.

Gibson, A.E., Noel, R.J., Herlihy, J.T. & Ward, W.F. (1989) Phenylarsine oxide inhibition of endocytosis: effects on asialofetuin internalization. *Am J Physiol*, **257**, C182–184.

Grati, M., Schneider, M.E., Lipkow, K., Strehler, E.E., Wenthold, R.J. & Kachar, B. (2006) Rapid turnover of stereocilia membrane proteins: evidence from the trafficking and mobility of plasma membrane Ca(2+)-ATPase 2. *J Neurosci*, **26**, 6386–6395.

Griesinger, C.B., Richards, C.D. & Ashmore, J.F. (2002) FM1-43 reveals membrane recycling in adult inner hair cells of the mammalian cochlea. *J Neurosci*, **22**, 3939–3952.

Griesinger, C.B., Richards, C.D. & Ashmore, J.F. (2004) Apical endocytosis in outer hair cells of the mammalian cochlea. *Eur J Neurosci*, **20**, 41–50.

Harasztosi, C., Badum, S. & Gummer, A.W. (2016) Vesicle traffic in the outer hair cell of the guinea-pig cochlea. In Santi, P.A. (ed) *Assoc. Res. Otolaryngol. Abs.*, San Diego, California, pp. 51.

Harasztosi, C. & Gummer, A.W. (2008) Position of calcium entry into the outer hair cell stereocilia. In Santi, P.A. (ed) *Assoc. Res. Otolaryngol. Abs.*, Phoenix, Arizona, pp. 223.

Harasztosi, C., Harasztosi, E. & Gummer, A.W. (2014) Membrane recycling at the subnuclear pole of the outer hair cell. In Karavitaki, K.D., Corey, D.P. (eds) *Mechanics of Hearing Workshop*. AIP Publishing LLC, Cape Sounio, Greece, pp. 030017-1–6.

Harasztosi, C., Klenske, E., Badum, S., Harasztosi, E. & Gummer, A.W. (2018) Double fluorescent labelling of a bipolar epithelial cell in vitro: The outer hair cell. *J Neurosci Methods*, **293**, 310–320.

Haugland, R.P. (2005) Probes for endocytosis, receptors and ion channels. In Spence, M.T.Z. (ed) *The Handbook (A Guide to Fluorescent Probes and Labeling Technologies)*, pp. 777–814.

Heissler, S.M., Selvadurai, J., Bond, L.M., Fedorov, R., Kendrick-Jones, J., Buss, F. & Manstein, D.J. (2012) Kinetic properties and small-molecule inhibition of human myosin-6. *FEBS Lett*, **586**, 3208–3214.

Helle, F. & Dubuisson, J. (2008) Hepatitis C virus entry into host cells. *Cell Mol Life Sci*, **65**, 100–112.

Hertzano, R., Shalit, E., Rzadzinska, A.K., Dror, A.A., Song, L., Ron, U., Tan, J.T., Shitrit, A.S., Fuchs, H., Hasson, T., Ben-Tal, N., Sweeney, H.L., de Angelis,

M.H., Steel, K.P. & Avraham, K.B. (2008) A Myo6 mutation destroys coordination between the myosin heads, revealing new functions of myosin VI in the stereocilia of mammalian inner ear hair cells. *PLoS Genet*, **4**, e1000207.

Hidalgo, I.J., Raub, T.J. & Borchardt, R.T. (1989) Characterization of the human colon carcinoma cell line (Caco-2) as a model system for intestinal epithelial permeability. *Gastroenterology*, **96**, 736–749.

Huang, G. & Santos-Sacchi, J. (1993) Mapping the distribution of the outer hair cell motility voltage sensor by electrical amputation. *Biophys J*, **65**, 2228–2236.

Hudspeth, A.J. (1989) How the ear's works work. *Nature*, **341**, 397–404.

Kachar, B., Battaglia, A. & Fex, J. (1997) Compartmentalized vesicular traffic around the hair cell cuticular plate. *Hear Res*, **107**, 102–112.

Kachar, B., Brownell, W.E., Altschuler, R. & Fex, J. (1986) Electrokinetic shape changes of cochlear outer hair cells. *Nature*, **322**, 365-368.

Kalinec, F., Holley, M.C., Iwasa, K.H., Lim, D.J. & Kachar, B. (1992) A membrane-based force generation mechanism in auditory sensory cells. *Proc Natl Acad Sci U S A*, **89**, 8671–8675.

Kaneko, T., Harasztosi, C., Mack, A.F. & Gummer, A.W. (2006) Membrane traffic in outer hair cells of the adult mammalian cochlea. *Eur J Neurosci*, **23**, 2712–2722.

Kelly, R.B. (1990) Microtubules, membrane traffic, and cell organization. *Cell*, **61**, 5–7.

Kirchhausen, T., Harrison, S.C., Chow, E.P., Mattaliano, R.J., Ramachandran, K.L., Smart, J. & Brosius, J. (1987a) Clathrin heavy chain: molecular cloning and complete primary structure. *Proc Natl Acad Sci U S A*, **84**, 8805–8809.

Kirchhausen, T., Scarmato, P., Harrison, S.C., Monroe, J.J., Chow, E.P., Mattaliano, R.J., Ramachandran, K.L., Smart, J.E., Ahn, A.H. & Brosius, J. (1987b) Clathrin light chains LCA and LCB are similar, polymorphic, and share repeated heptad motifs. *Science*, **236**, 320–324.

Koning, A.J., Lum, P.Y., Williams, J.M. & Wright, R. (1993) DiOC6 staining reveals organelle structure and dynamics in living yeast cells. *Cell Motil Cytoskeleton*, **25**, 111–128.

Kutsuna, N. & Hasezawa, S. (2002) Dynamic organization of vacuolar and microtubule structures during cell cycle progression in synchronized tobacco BY-2 cells. *Plant Cell Physiol*, **43**, 965–973.

Langford, G.M. (1995) Actin- and microtubule-dependent organelle motors: interrelationships between the two motility systems. *Curr Opin Cell Biol*, **7**, 82–88.

LeMasurier, M. & Gillespie, P.G. (2005) Hair-cell mechanotransduction and cochlear amplification. *Neuron*, **48**, 403–415.

Lim, J.P. & Gleeson, P.A. (2011) Macropinocytosis: an endocytic pathway for internalising large gulps. *Immunol Cell Biol*, **89**, 836–843.

Luttrell, L.M., Daaka, Y., Della Rocca, G.J. & Lefkowitz, R.J. (1997) G protein-coupled receptors mediate two functionally distinct pathways of tyrosine phosphorylation in rat 1a fibroblasts. Shc phosphorylation and receptor endocytosis correlate with activation of Erk kinases. *J Biol Chem*, **272**, 31648–31656.

Mamdouh, Z., Giocondi, M.C., Laprade, R. & Le Grimellec, C. (1996) Temperature dependence of endocytosis in renal epithelial cells in culture. *Biochim Biophys Acta*, **1282**, 171–173.

Mammano, F., Bortolozzi, M., Ortolano, S. & Anselmi, F. (2007) Ca^{2+} signaling in the inner ear. *Physiology (Bethesda)*, **22**, 131–144.

Marx, A., Hoenger, A. & Mandelkow, E. (2009) Structures of kinesin motor proteins. *Cell Motil Cytoskeleton*, **66**, 958–966.

Matteoli, M., Verderio, C., Rossetto, O., Iezzi, N., Coco, S., Schiavo, G. & Montecucco, C. (1996) Synaptic vesicle endocytosis mediates the entry of tetanus neurotoxin into hippocampal neurons. *Proc Natl Acad Sci U S A*, **93**, 13310–13315.

Mays, R.W., Beck, K.A. & Nelson, W.J. (1994) Organization and function of the cytoskeleton in polarized epithelial cells: a component of the protein sorting machinery. *Curr Opin Cell Biol*, **6**, 16–24.

Menard, S., Cerf-Bensussan, N. & Heyman, M. (2010) Multiple facets of intestinal permeability and epithelial handling of dietary antigens. *Mucosal Immunol*, **3**, 247-259.

Meng, W., Mushika, Y., Ichii, T. & Takeichi, M. (2008) Anchorage of microtubule minus ends to adherens junctions regulates epithelial cell-cell contacts. *Cell*, **135**, 948–959.

Meyer, J., Mack, A.F. & Gummer, A.W. (2001) Pronounced infracuticular endocytosis in mammalian outer hair cells. *Hear Res*, **161**, 10–22.

Meyers, J.R., MacDonald, R.B., Duggan, A., Lenzi, D., Standaert, D.G., Corwin, J.T. & Corey, D.P. (2003) Lighting up the senses: FM1-43 loading of sensory cells through nonselective ion channels. *J Neurosci*, **23**, 4054–4065.

Miaczynska, M. & Stenmark, H. (2008) Mechanisms and functions of endocytosis. *J Cell Biol*, **180**, 7–11.

Moser, T. & Beutner, D. (2000) Kinetics of exocytosis and endocytosis at the cochlear inner hair cell afferent synapse of the mouse. *Proc Natl Acad Sci U S A*, **97**, 883–888.

Moussa, R. (2012) *Eine kritische Evaluierung FRET-basierter Biosensoren als Werkzeuge für die quantitative Metabolitanalytik*. Forschungszentrum Jülich.

Mundigl, O., Matteoli, M., Daniell, L., Thomas-Reetz, A., Metcalf, A., Jahn, R. & De Camilli, P. (1993) Synaptic vesicle proteins and early endosomes in cultured hippocampal neurons: differential effects of Brefeldin A in axon and dendrites. *J Cell Biol*, **122**, 1207–1221.

Nadol, J.B., Jr. (1983) Serial section reconstruction of the neural poles of hair cells in the human organ of Corti. II. outer hair cells. *Laryngoscope*, **93**, 780–791.

Nakata, T., Terada, S. & Hirokawa, N. (1998) Visualization of the dynamics of synaptic vesicle and plasma membrane proteins in living axons. *J Cell Biol*, **140**, 659–674.

Nunez, M.T., Tapia, V. & Arredondo, M. (1996) Intestinal epithelia (Caco-2) cells acquire iron through the basolateral endocytosis of transferrin. *J Nutr*, **126**, 2151–2158.

Pettit, E.J. & Hallett, M.B. (1998) Two distinct Ca^{2+} storage and release sites in human neutrophils. *J Leukoc Biol*, **63**, 225–232.

Plinkert, P.K., Mohler, H. & Zenner, H.P. (1989) A subpopulation of outer hair cells possessing GABA receptors with tonotopic organization. *Arch Otorhinolaryngol*, **246**, 417–422.

Preyer, S., Hemmert, W., Pfister, M., Zenner, H.P. & Gummer, A.W. (1994) Frequency response of mature guinea-pig outer hair cells to stereociliary displacement. *Hear Res*, **77**, 116–124.

Raphael, Y., Athey, B.D., Wang, Y., Lee, M.K. & Altschuler, R.A. (1994) F-actin, tubulin and spectrin in the organ of Corti: comparative distribution in different cell types and mammalian species. *Hear Res*, **76**, 173–187.

Rothberg, K.G., Heuser, J.E., Donzell, W.C., Ying, Y.S., Glenney, J.R. & Anderson, R.G. (1992) Caveolin, a protein component of caveolae membrane coats. *Cell*, **68**, 673–682.

Ryan, T.A., Smith, S.J. & Reuter, H. (1996) The timing of synaptic vesicle endocytosis. *Proc Natl Acad Sci U S A*, **93**, 5567–5571.

Safieddine, S. & Wenthold, R.J. (1999) SNARE complex at the ribbon synapses of cochlear hair cells: analysis of synaptic vesicle- and synaptic membrane-associated proteins. *Eur J Neurosci*, **11**, 803–812.

Saito, K. (1983) Fine structure of the sensory epithelium of guinea-pig organ of Corti: subsurface cisternae and lamellar bodies in the outer hair cells. *Cell Tissue Res*, **229**, 467–481.

Siegel, J.H. & Brownell, W.E. (1986) Synaptic and Golgi membrane recycling in cochlear hair cells. *J Neurocytol*, **15**, 311–328.

Smith, C.B. & Betz, W.J. (1996) Simultaneous independent measurement of endocytosis and exocytosis. *Nature*, **380**, 531–534.

Smith, S.M., Renden, R. & von Gersdorff, H. (2008) Synaptic vesicle endocytosis: fast and slow modes of membrane retrieval. *Trends Neurosci*, **31**, 559–568.

So, P.T., Dong, C.Y., Masters, B.R. & Berland, K.M. (2000) Two-photon excitation fluorescence microscopy. *Annu Rev Biomed Eng*, **2**, 399–429.

Spoendlin, H. (1972) Innervation densities of the cochlea. *Acta Otolaryngol*, **73**, 235–248.

Svoboda, K. & Yasuda, R. (2006) Principles of two-photon excitation microscopy and its applications to neuroscience. *Neuron*, **50**, 823–839.

Tan, J.S., Seow, C.J., Goh, V.J. & Silver, D.L. (2014) Recent advances in understanding proteins involved in lipid droplet formation, growth and fusion. *J Genet Genomics*, **41**, 251–259.

Terasaki, M. (1989) Fluorescent labeling of endoplasmic reticulum. *Methods Cell Biol*, **29**, 125–135.

Terasaki, M. & Reese, T.S. (1992) Characterization of endoplasmic reticulum by co-localization of BiP and dicarbocyanine dyes. *J Cell Sci*, **101 (Pt 2)**, 315–322.

Thiam, A.R., Farese, R.V., Jr. & Walther, T.C. (2013) The biophysics and cell biology of lipid droplets. *Nat Rev Mol Cell Biol*, **14**, 775–786.

Toba, S., Watanabe, T.M., Yamaguchi-Okimoto, L., Toyoshima, Y.Y. & Higuchi, H. (2006) Overlapping hand-over-hand mechanism of single molecular motility of cytoplasmic dynein. *Proc Natl Acad Sci U S A*, **103**, 5741–5745.

Traub, L.M. (2003) Sorting it out: AP-2 and alternate clathrin adaptors in endocytic cargo selection. *J Cell Biol*, **163**, 203–208.

Tuma, P. & Hubbard, A.L. (2003) Transcytosis: crossing cellular barriers. *Physiol Rev*, **83**, 871–932.

Tumbarello, D.A., Kendrick-Jones, J. & Buss, F. (2013) Myosin VI and its cargo adaptors - linking endocytosis and autophagy. *J Cell Sci*, **126**, 2561–2570.

Tuxworth, R.I. & Titus, M.A. (2000) Unconventional myosins: anchors in the membrane traffic relay. *Traffic*, **1**, 11–18.

Urrutia, R.A. & Kalinec, F. (2015) Biology and pathobiology of lipid droplets and their potential role in the protection of the organ of Corti. *Hear Res*, **330**, 26–38.

Wells, A.L., Lin, A.W., Chen, L.Q., Safer, D., Cain, S.M., Hasson, T., Carragher, B.O., Milligan, R.A. & Sweeney, H.L. (1999) Myosin VI is an actin-based motor that moves backwards. *Nature*, **401**, 505–508.

Wu, L.G., Ryan, T.A. & Lagnado, L. (2007) Modes of vesicle retrieval at ribbon synapses, calyx-type synapses, and small central synapses. *J Neurosci*, **27**, 11793–11802.

Xu, J., McNeil, B., Wu, W., Nees, D., Bai, L. & Wu, L.G. (2008) GTP-independent rapid and slow endocytosis at a central synapse. *Nat Neurosci*, **11**, 45–53.

Zenner, H.P. (1986) Motile responses in outer hair cells. *Hear Res*, **22**, 83–90.

Zheng, J., Shen, W., He, D.Z., Long, K.B., Madison, L.D. & Dallos, P. (2000) Prestin is the motor protein of cochlear outer hair cells. *Nature*, **405**, 149–155.

8 Erklärung zum Eigenanteil

Die Arbeit wurde in der Universitäts-HNO-Klinik Tübingen, Sektion Physiologische Akustik und Kommunikation, unter Betreuung von Professor Dr. A. W. Gummer durchgeführt.
Die Konzeption der Studie erfolgte in Zusammenarbeit mit Prof. Dr. Prof. h.c. A. W. Gummer (Doktorvater) und Dr. C. Harasztosi, (Betreuer).
Sämtliche Versuche wurden nach Einarbeitung durch Dr. C. Harasztosi von mir eigenständig durchgeführt.
Die statistische Auswertung erfolgte nach Anleitung durch Dr. C. Harasztosi durch mich.
Ich versichere, das Manuskript selbständig verfasst zu haben und keine weiteren als die von mir angegebenen Quellen verwendet zu haben.

9 Danksagung

Mein Dank gebührt Prof. Dr. Prof. h.c. Anthony Gummer für die exzellente Supervision während der Doktorarbeit und den stets hilfreichen Anmerkungen.
Ebenso möchte ich Dr. Csaba Harasztosi für die Einführung in die faszinierende Arbeit mit dem konfokalen Mikroskop sowie dem Multhiphotonmikroskop danken.
Durch diese beiden Personen entdeckte ich die Freude am wissenschaftlichen Arbeiten.

10 Veröffentlichungen

Teile der vorliegenden Dissertationsschrift wurden bereits in den folgenden Publikationen veröffentlicht:

Harasztosi, C., Klenske, E., Badum, S., Harasztosi, E. & Gummer, A.W. (2018)
Double fluorescent labelling of a bipolar epithelial cell in vitro: The outer hair cell. *J Neurosci Methods*, **293**, 310–320.

Harasztosi, C., Klenske, E. & Gummer, A.W. (2021)
Vesicle traffic in the outer hair cell. *Eur J Neurosci,* **54**, 4755–4767.